DNA supercoiling restricts the transcriptional bursting of neighboring eukaryotic genes

Heta Patel, Stefano Coppola, Wim Pomp, Umberto Aiello, Ineke Brouwer, Domenico Libri, Tineke Lenstra

▶ **To cite this version:**

Heta Patel, Stefano Coppola, Wim Pomp, Umberto Aiello, Ineke Brouwer, et al.. DNA supercoiling restricts the transcriptional bursting of neighboring eukaryotic genes. Molecular Cell, 2023, 83 (10), pp.1573-1587.e8. 10.1016/j.molcel.2023.04.015 . hal-04916557

HAL Id: hal-04916557
https://hal.science/hal-04916557v1

Submitted on 28 Jan 2025

HAL is a multi-disciplinary open access archive for the deposit and dissemination of scientific research documents, whether they are published or not. The documents may come from teaching and research institutions in France or abroad, or from public or private research centers.

L'archive ouverte pluridisciplinaire **HAL**, est destinée au dépôt et à la diffusion de documents scientifiques de niveau recherche, publiés ou non, émanant des établissements d'enseignement et de recherche français ou étrangers, des laboratoires publics ou privés.

Distributed under a Creative Commons Attribution - NonCommercial - NoDerivatives 4.0 International License

Molecular Cell

Article

DNA supercoiling restricts the transcriptional bursting of neighboring eukaryotic genes

Graphical abstract

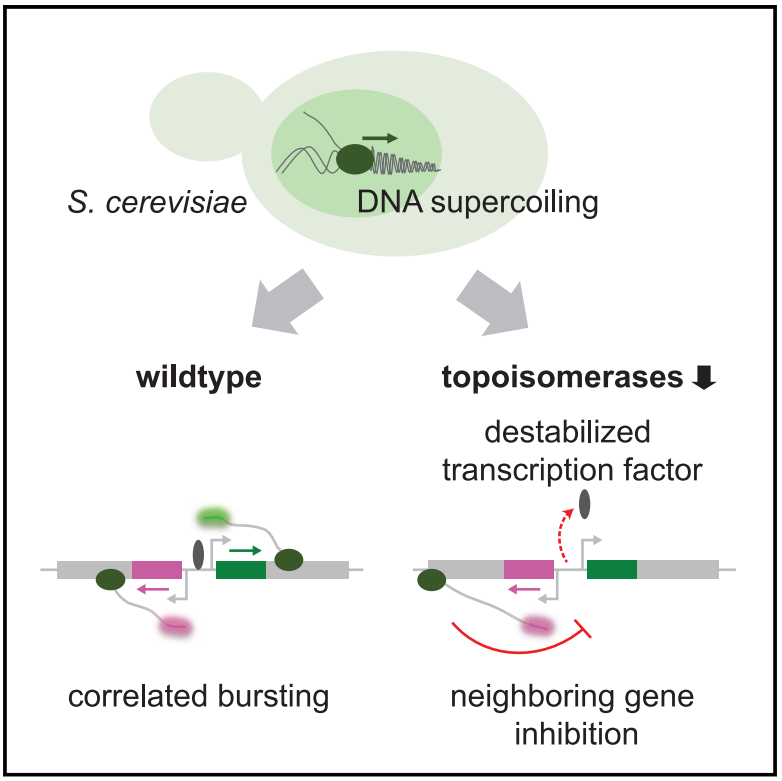

Authors

Heta P. Patel, Stefano Coppola, Wim Pomp, Umberto Aiello, Ineke Brouwer, Domenico Libri, Tineke L. Lenstra

Correspondence

t.lenstra@nki.nl

In brief

Patel et al. use single-molecule visualization of transcription of neighboring genes at the *GAL* locus in budding yeast to elucidate how DNA supercoils regulate transcription dynamics in eukaryotes. Accumulation of DNA supercoils from transcription impedes transcription at adjacent genes, but wild-type yeast prevents inhibition by sufficient supercoiling release.

Highlights

- Transcription of neighboring *GAL* genes is coupled, and supercoils impede coupling
- Buildup of supercoils from transcription inhibits transcription at adjacent genes
- Inhibition occurs through destabilized DNA binding of the transcription factor
- Wild-type yeast contains sufficient topoisomerase levels to prevent inhibition

Patel et al., 2023, Molecular Cell *83*, 1573–1587
May 18, 2023 © 2023 The Author(s). Published by Elsevier Inc.
https://doi.org/10.1016/j.molcel.2023.04.015

CellPress

Molecular Cell

CellPress
OPEN ACCESS

Article

DNA supercoiling restricts the transcriptional bursting of neighboring eukaryotic genes

Heta P. Patel,[1] Stefano Coppola,[1] Wim Pomp,[1] Umberto Aiello,[2,4] Ineke Brouwer,[1] Domenico Libri,[2,3] and Tineke L. Lenstra[1,5,*]

[1]Division of Gene Regulation, The Netherlands Cancer Institute, Oncode Institute, 1066CX Amsterdam, the Netherlands
[2]Université Paris Cité, CNRS, Institut Jacques Monod, 75013 Paris, France
[3]Present address: Institut de Génétique Moléculaire de Montpellier, Univ Montpellier, CNRS, Montpellier, France
[4]Present address: Department of Genetics, Stanford University School of Medicine, Stanford, CA, USA
[5]Lead contact
*Correspondence: t.lenstra@nki.nl
https://doi.org/10.1016/j.molcel.2023.04.015

SUMMARY

DNA supercoiling has emerged as a major contributor to gene regulation in bacteria, but how DNA supercoiling impacts transcription dynamics in eukaryotes is unclear. Here, using single-molecule dual-color nascent transcription imaging in budding yeast, we show that transcriptional bursting of divergent and tandem *GAL* genes is coupled. Temporal coupling of neighboring genes requires rapid release of DNA supercoils by topoisomerases. When DNA supercoils accumulate, transcription of one gene inhibits transcription at its adjacent genes. Transcription inhibition of the *GAL* genes results from destabilized binding of the transcription factor Gal4. Moreover, wild-type yeast minimizes supercoiling-mediated inhibition by maintaining sufficient levels of topoisomerases. Overall, we discover fundamental differences in transcriptional control by DNA supercoiling between bacteria and yeast and show that rapid supercoiling release in eukaryotes ensures proper gene expression of neighboring genes.

INTRODUCTION

During transcription, the movement of RNA polymerase along the DNA generates negative supercoils behind RNA polymerase and positive supercoils in front, as described by the twin-supercoiled-domain model.[1–3] Transcription-generated supercoils can, in turn, enhance or impede the transcriptional process: negative supercoils facilitate transcription initiation by enabling promoter melting and enhancing the binding of regulatory factors, whereas positive supercoils aid the elongation of RNA polymerases by destabilizing DNA-bound proteins.[4–9] However, excessive negative or positive supercoils can also repress transcription.[10–14] In *E. coli*, the topoisomerase gyrase is limiting, such that at highly transcribed genes, the dynamic accumulation and release of positive supercoils stochastically switch genes off and on, thereby causing transcriptional bursting.[10] Whether eukaryotic topoisomerase levels are limiting and how positive and negative DNA supercoiling control transcriptional bursting in eukaryotes is still unknown.

Transcription-generated supercoils can propagate along the DNA and may activate or deactivate adjacent genes. For multiple bacterial species, negative supercoils generated behind polymerase enhance transcription of upstream divergent genes, whereas positive supercoils in front of polymerase inhibit the transcription of downstream tandem and convergent genes.[15–19] Similar mechanisms were proposed in eukaryotes, but direct *in vivo* evidence is lacking.[20–27] In contrast to bacterial DNA, eukaryotic DNA is wrapped in nucleosomes, which may buffer excess positive supercoils to limit their dissipation.[28,29] However, chromatin does not absorb negative supercoils.[30] Accordingly, negative supercoils propagate up to 1.5 kb around the transcription start site of transcribed genes.[23] Whether *in vivo* negative supercoils enhance the transcription of divergent genes and whether positive supercoils are efficiently buffered by nucleosomes to prevent the inhibition of tandem and convergent genes remain unclear. Additionally, since these previous studies relied on population-based transcription assays, it is unclear whether the transcriptional bursting of adjacent genes is temporally coupled in single cells and how DNA supercoils affect their temporal relationship.

Supercoiling-mapping studies observed that gene bodies are positively supercoiled, and promoters are negatively supercoiled.[23,31–33] Promoters are maintained in a negatively supercoiled state by restricting topoisomerase TOP1 activity to gene bodies.[34] In addition, mammalian genomes contain large negatively supercoiled domains of actively transcribed genes.[33] However, since the mapping of supercoils at the single-cell level is technically challenging, little is known about the differences in supercoiling states between cells at a single time point or how supercoiling dynamics affect the transcription dynamics of single eukaryotic cells over time.

This is an open access article under the CC BY-NC-ND license (http://creativecommons.org/licenses/by-nc-nd/4.0/).

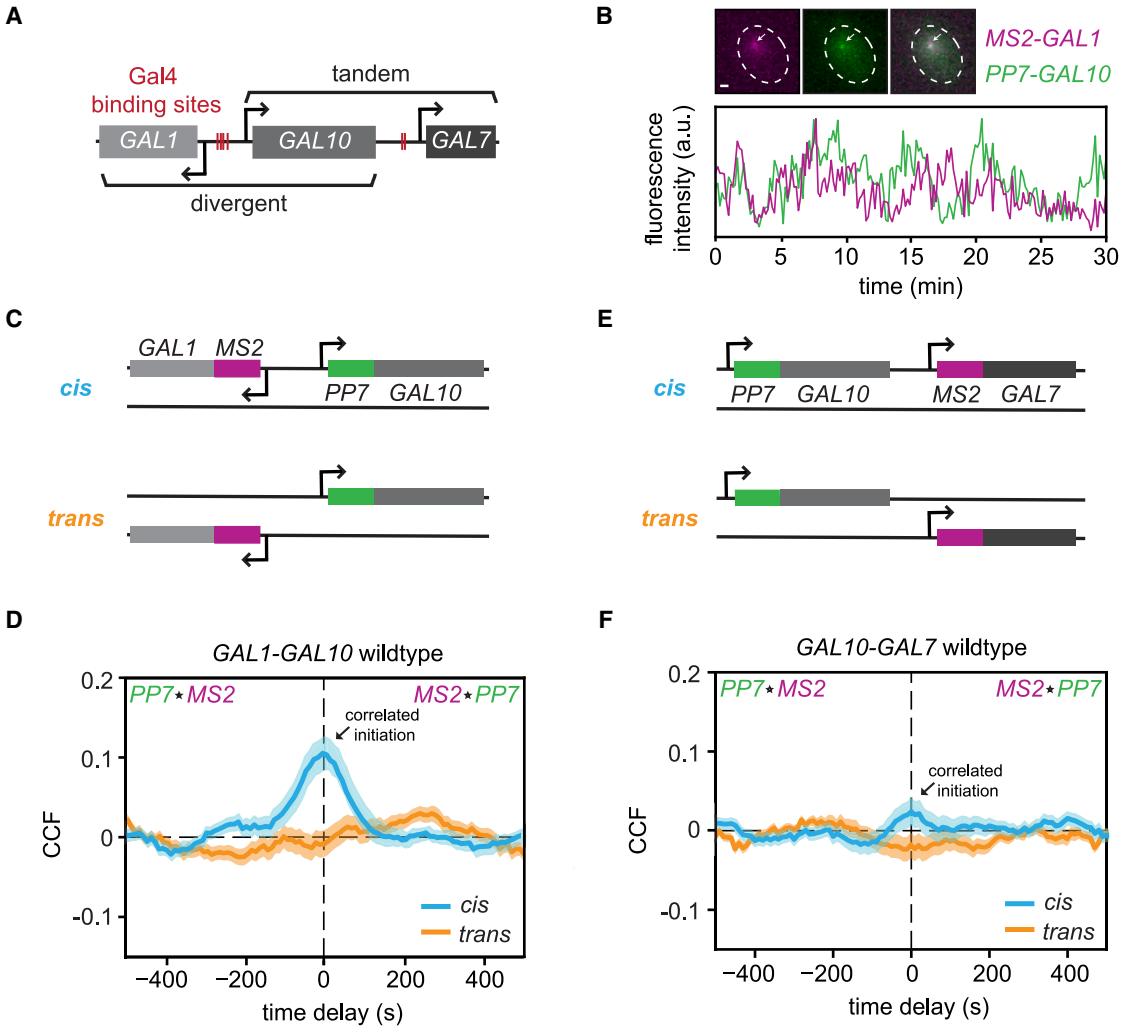

Figure 1. Transcriptional bursting of the divergent and tandem *GAL* genes is temporally coupled

(A) Schematic of *GAL* gene cluster in yeast. Red lines indicate the binding sites of the transcription factor, Gal4. The gene lengths of *GAL1*, *GAL10*, and *GAL7* are approximately 1.5, 2.1, and 1.1 kb, respectively, with intergenic distances of 669 and 726 bp. All three genes are highly transcriptionally active in galactose-containing media and produce high levels of DNA supercoils.[31] In galactose, the antisense transcripts at this locus are not transcribed.[35]

(B) Example images of *MS2-GAL1* (magenta), *PP7-GAL10* (green), and merged (gray) transcription sites (TSs), indicated by arrows (top). Scale bars, 1 μm. Example traces of the quantified fluorescence intensities (arbitrary units) of the *MS2-GAL1* and *PP7-GAL10* TSs (bottom).

(C) Nascent transcription of *GAL1-GAL10* is visualized either on the same allele (*cis*) or different alleles (*trans*).

(D) *MS2-PP7* cross-correlation of *GAL1-GAL10* in the *cis* (blue, n = 179 cells) and *trans* (orange, n = 162 cells) configuration. Shaded area indicates SEM. MS2★PP7 indicates the CCF of MS2(t) to PP7(t+τ) and PP7★MS2 of MS2(t−τ) to PP7(t).

(E) Same as (C) for *GAL10-GAL7*.

(F) Same as (D) for *GAL10-GAL7*. *Cis*: n = 148 cells; *trans*: n = 125 cells.

See also Figures S1 and S2 and Video S1.

In this study, we used the closely positioned and highly expressed divergent (*GAL1-GAL10*) and tandem (*GAL10-GAL7*) gene pairs of the *GAL* gene cluster in *S. cerevisiae* to investigate how DNA supercoiling affects transcriptional bursting of neighboring eukaryotic genes (Figure 1A). Using single-molecule dual-color imaging, we found that transcriptional bursting of the *GAL* gene pairs is temporally correlated inside single cells and that yeast topoisomerases are essential for maintaining the correlation. Topoisomerase degradation results in transcription inhibition at neighboring genes that is likely a consequence of the accumulation of both positive and negative supercoils. The resulting transcription inhibition is caused by destabilized binding of the transcription factor (TF) Gal4. Moreover, we find that wild-type (WT) budding yeast has sufficient concentrations of topoisomerases to minimize the inhibition of DNA supercoiling on transcription, implying that DNA supercoils play different regulatory roles on gene transcription in prokaryotes versus eukaryotes.

CellPress
OPEN ACCESS

RESULTS

Transcriptional bursting of the divergent and tandem *GAL* genes is temporally coupled

To understand how neighboring *GAL* genes are dynamically transcribed inside single cells, we first visualized nascent transcription of the divergent *GAL* gene pair with single-molecule resolution in live cells by inserting 12xMS2V6 repeats and 14xPP7 repeats at the 5′ of *GAL1* and *GAL10*, respectively (Figures 1B and 1C).[36,37] Upon transcription, these repeats form loops that are specifically bound by the fluorescently tagged MS2 and PP7 coat proteins, allowing for nascent RNA visualization at the endogenous loci in living cells. The divergent genes were labeled on the same chromosome (*cis* configuration) or on two different chromosomes (*trans* configuration) (Figure 1C) to distinguish between local environment effects and extrinsic noise effects, such as correlations generated by cell-to-cell variations.

To determine whether the transcriptional bursting of the *GAL1-GAL10* genes was temporally coupled, we imaged live cells that were induced with galactose, quantified the intensities of the *MS2-GAL1* and *PP7-GAL10* transcription sites (TSs), and computed the *MS2-PP7* cross-correlation function (CCF) (Figures 1B, 1D, and S1A–S1C). The CCF of the *MS2* and *PP7* time traces was calculated by shifting one trace with respect to another trace by defined time delays, yielding a measure of similarity between *MS2-GAL1* and *PP7-GAL10* signals at various time delays. The *MS2-PP7* CCF of the *cis*-labeled genes displayed a defined peak at time delay zero, indicating that *GAL1* and *GAL10* initiate together more than expected by random chance (Figure 1D). The CCF decayed to zero at time delays of approximately −100 and +100 s, which was in accordance with the decay of *GAL1* and *GAL10* from the auto-correlation functions (ACFs) (Figures S1B and S1C), indicating that after a simultaneous burst, *GAL1* and *GAL10* transcription is uncorrelated. The CCF of the *trans*-labeled divergent genes yielded a flat line (Figure 1D), as expected for independently expressed, uncorrelated genes on different chromosomes. To understand the magnitude of the correlation at zero time delay, we quantified the normalized transcriptional overlap, which represents the percentage of co-occurring *GAL1-GAL10* transcription events when *GAL10* is active (STAR Methods).[38] Although we observed a substantial random transcriptional overlap (66% ± 2%) for the *trans* control, the overlap of the *cis* configuration was significantly higher (79% ± 1%) (Figure S2C), demonstrating that the transcription of the divergent genes is more correlated in the *cis* configuration than in the *trans* and that transcription initiation of divergent genes on the same chromosome is temporally coupled.

Because the transcriptional overlap of the *trans* was already substantial, we investigated whether the difference between the *cis* and *trans* overlap would increase in conditions with lower galactose concentrations with reduced transcriptional activity, where the random overlap may be lower (Figures S1A–S1C). Despite the reduced transcriptional activity, both the *cis* and the *trans* transcriptional overlaps remained the same (Figures S2A–S2C), indicating that the overlap is similar across conditions and confirming that the normalized transcriptional overlap is independent of the transcriptional activity.

The *cis* and *trans* correlations were corroborated using single-molecule RNA fluorescence *in situ* hybridization (smFISH) with probes hybridizing to the MS2 and PP7 loops.[39] As a measure for correlated transcription, we computed the Pearson correlation coefficient of the nascent transcript number at the *MS2-GAL1* and *PP7-GAL10* TSs across thousands of transcriptionally active cells (Figure S2D). Consistent with the live-cell results, *GAL1-GAL10* transcription shows a higher Pearson correlation in the *cis* (R = 0.20 ± 0.02) than in the *trans* (R = 0.12 ± 0.02) configuration. When positioned on the same chromosome, the divergent *GAL1-GAL10* genes thus initiate simultaneously, more than by random chance.

Next, the same approach was used for the tandem *GAL10-GAL7* genes (Figures 1E, S1D–S1F, S2E, and S2F). The *cis*-labeled tandem genes are weakly correlated at time delay zero (Figure 1F) with a transcriptional overlap that is 6.0% ± 0.3% higher than the *trans* control (Figure S2E). This modest difference could not be confirmed by smFISH (Figure S2F), presumably because it is obscured by extrinsic noise. Overall, live-cell imaging and smFISH indicate that transcription of the divergent and tandem *GAL* gene pairs in WT yeast is temporally coupled.

Degradation of topoisomerases results in refractory periods

In yeast, transcription-generated supercoiling levels are managed by topoisomerases, Top1 and Top2, which can release both positive and negative supercoils.[40] To investigate how DNA supercoiling affects the transcription dynamics and the temporal correlation of the *GAL* gene pairs, we perturbed DNA supercoiling levels by conditionally degrading endogenous Top1 and Top2 using the auxin-inducible degron system[41] (Figure 2A). Strains containing degron-tagged Top1 and Top2, without OsTIR1 expression, showed a similar *GAL1-GAL10* correlation as WT, suggesting that tagging does not influence their function (Figure S2D). Homozygous expression of OsTIR1, even without the addition of auxin (−IAA), resulted in basal degradation (44% ± 1%) of the degron-tagged topoisomerases, as measured using the cMyc-tag on Top2 (Figures S2G and S2H). Top1 did not contain a cMyc-tag to monitor its degradation, but since the degron tag was the same, we assumed that its degradation was similar. The addition of auxin (+IAA) resulted in almost complete degradation (89% ± 2%) within 15 min (Figures S2G and S2H). We will refer to the basal and complete degradation conditions as partial (−IAA) and full (+IAA) topoisomerase degradation.

To understand how DNA supercoiling affects the transcription dynamics of the *GAL* genes, we performed live-cell imaging of *GAL1-GAL10* and *GAL10-GAL7* transcription on partial and full topoisomerase degradation (Figures S1A and S1D). Both topoisomerase degradation conditions resulted in a complete loss of *GAL* gene transcription in a large fraction of the population (Figures S2I and S2J). The active fraction expressing both *GAL1* and *GAL10* on topoisomerase degradation is lower in the *trans* than in the *cis* configuration (Figure S2I), suggesting that transcription activation may be impaired at divergent genes with different gene lengths from MS2/PP7 addition. In subsequent analysis, only transcriptionally active cells were analyzed, but these represented only 30% of the population in some conditions. In these active cells, transcription levels were up to 50%

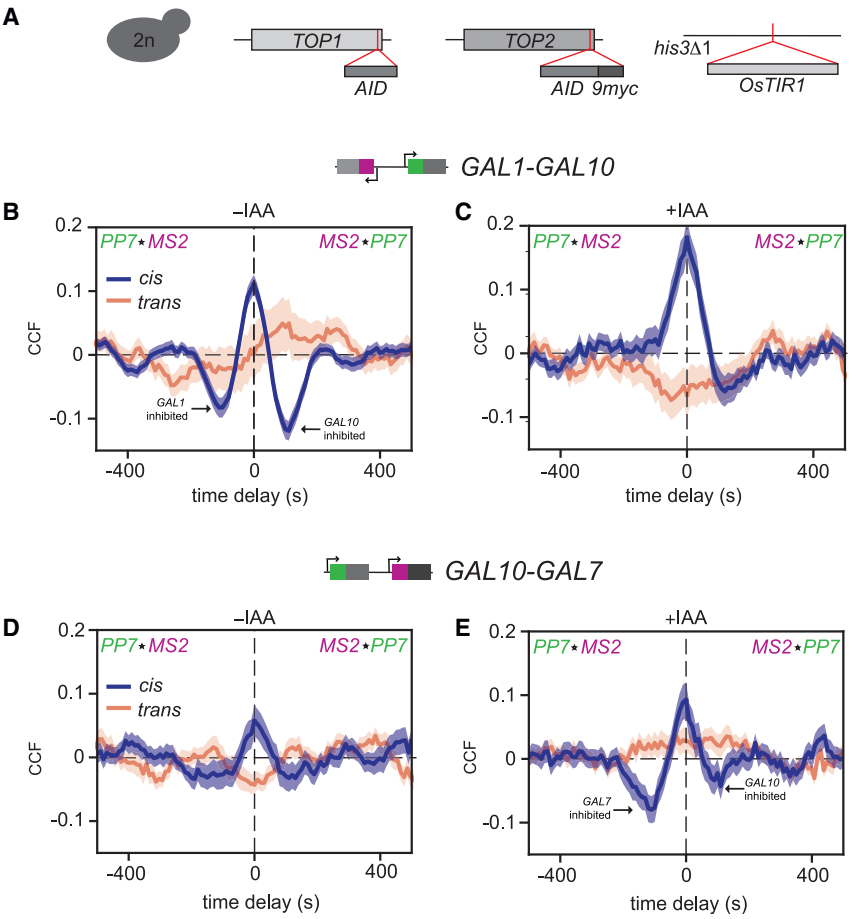

Figure 2. Degradation of topoisomerases results in refractory periods

(A) Schematic depicting the homozygous tagging of diploid yeast (2n) of endogenous *TOP1* and *TOP2* with an auxin-inducible degron, and homozygous *OsTIR1* insertion at the *his3Δ1* locus.

(B and C) *MS2-PP7* cross-correlation of the *GAL1-GAL10* in cells without (−IAA, left, n = 214 cells [*cis*], n = 126 cells [*trans*]) and with auxin (+IAA, right, n = 158 cells [*cis*], n = 112 cells [*trans*]) for the *cis* (dark blue) and *trans* (orange). Arrows indicate example valleys indicating refractory periods. Shaded area indicates SEM.

(D and E) Same as (B) and (C) for *GAL10-GAL7*. −IAA: n = 118 cells (*cis*), 102 cells (*trans*), +IAA: n = 143 cells (*cis*), n = 128 cells (*trans*).

See also Figures S1 and S2.

reduced after topoisomerase degradation, as measured from the inverse ACF amplitudes (Figure 3A). Topoisomerase degradation thus causes a large reduction in *GAL* gene transcription in the population.

Next, we explored how topoisomerase degradation affected the *GAL* gene coupling by calculating the CCFs. For *GAL1* and *GAL10*, partial topoisomerase degradation introduced valleys in the CCF around −100 and +100 s time delays that were not present in the *trans* (Figure 2B). These valleys indicate that 100 s after a correlated burst, simultaneous transcription of the two genes is observed less often than expected by random chance, suggesting that supercoils that accumulate from transcription inhibit subsequent transcription of its neighbor. Such periods of lower transcription initiation rates immediately after a transcriptional burst have been referred to as refractory periods.[42–44] In this manuscript, we employ the same nomenclature, regardless of whether the refractory period follows the transcription of the gene itself or neighboring genes. A *GAL1* transcriptional burst, either alone or together with *GAL10*, thus causes a refractory period for *GAL10* and vice versa. The CCF also showed recurring peaks every 200 s, indicating periodicity (Figure 2B), likely resulting from the refractory period. Similar but weaker valleys were observed in the ACFs, most prominently for *GAL10*, indicating *GAL10* transcription may also weakly inhibit itself (Figures S1B and S1C). On full topoisomerase degradation, the refractory periods and periodicity for *GAL1-GAL10* were partially alleviated (Figure 2C), possibly due to the concurrent reduction in the transcriptional activity of all *GAL* genes (Figure 3A). As bursts become less frequent (Figure S2M), inhibition from a neighboring gene is expected to interfere less with transcription patterns. In both partial and full depletion conditions, inhibition was stronger for *GAL10* than for *GAL1* (Figures 2B and 2C).

For *GAL10-GAL7*, similar refractory periods were observed, with especially strong *GAL7* inhibition after full topoisomerase degradation (Figures 2D and 2E). Because of the well-established inhibitory role of positive supercoils, we expect that positive supercoils generated from *GAL10* elongation may inhibit subsequent *GAL7* initiation.[10,19,32] Interestingly, a similar but much weaker valley at −100 s delay is already visible in WT (Figure 1F), suggesting that WT topoisomerase levels are just sufficient to minimize supercoiling-mediated inhibition. Overall, these data indicate that topoisomerase degradation causes refractory periods where transcription of a *GAL* gene inhibits subsequent transcription at neighboring genes.

Because the inhibition effects appear dependent on topoisomerase concentration, we constructed strains with heterozygous (1xOsTIR1) instead of homozygous (2xOsTIR1) OsTIR1 expression to explore the concentration dependence further. In these strains, both Top1 and Top2 were cMyc-tagged, confirming that both were equally degraded (Figures S2G and S2H). Heterozygous rather than homozygous OsTIR1 expression not only reduced the basal degradation to 23% ± 1% but also showed slightly less degradation on auxin addition (Figure S2H). These strains yielded intermediate phenotypes (Figures S2N and S2O). For *GAL1-GAL10*, refractory periods were stronger at partial than at full topoisomerase degradation with more *GAL10* than *GAL1* inhibition (Figures S1B, S1C, and S2N), whereas for *GAL7-GAL10*, refractory periods were stronger at full degradation with more *GAL7* than *GAL10* inhibition (Figures S1E, S1F, and S2O). Overall, these results indicate that topoisomerases are important

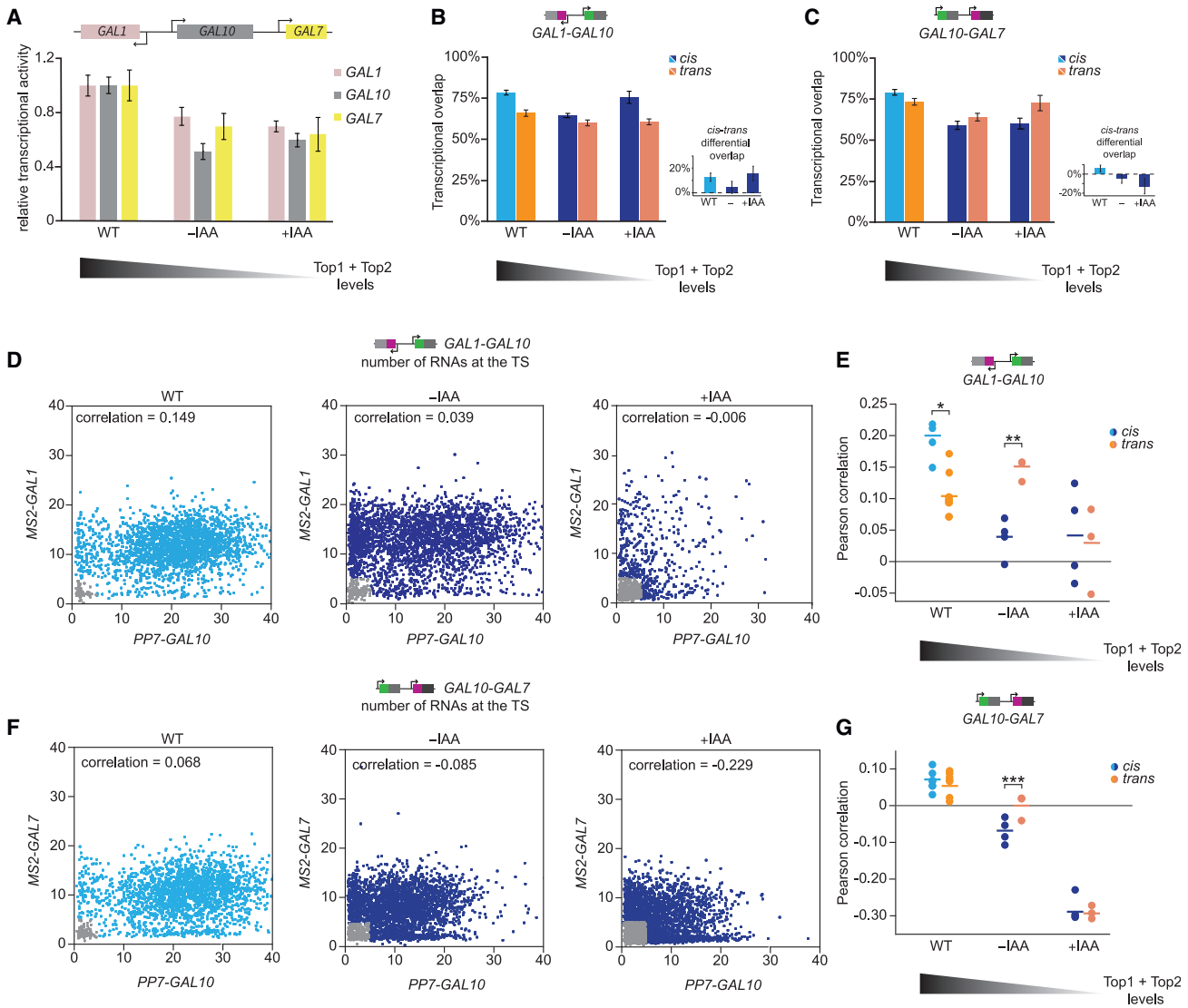

Figure 3. Degradation of topoisomerases reduces the simultaneous initiation of neighboring genes

(A) Relative transcriptional activity of *GAL1*, *GAL10*, and *GAL7* in WT and partial (−IAA) and full (+IAA) topoisomerase degradation conditions, calculated by taking the inverse of the ACF amplitudes. WT is normalized to 1. Error bars indicate SEM.

(B and C) Transcriptional overlap of *cis* and *trans* conditions for WT, −IAA, and +IAA conditions for (B) *GAL1-GAL10* and (C) *GAL10-GAL7* computed from the CCF at zero time delay from live-cell experiments. Error bars indicate SEM. The insets show the *cis-trans* overlap difference for each condition.

(D) Example scatterplots of the number of nascent transcripts at *MS2-GAL1* and *PP7-GAL10* TSs, determined by smFISH, in WT (left, n = 2,602 cells), −IAA (middle, n = 3,096 cells), and +IAA (right, n = 1,112 cells) for the *cis*. Each datapoint represents a cell. Scatter plots show one representative replicate out of multiple replicate experiments (n = 4;4;4, from left to right). From these plots, the *GAL1-GAL10* active fraction (Figure S2P) and the *GAL1-GAL10* Pearson correlation was calculated (E). Gray data points represent transcriptionally inactive cells that were excluded from the Pearson correlation coefficient calculation.

(E) Pearson correlation coefficients of *GAL1-GAL10* nascent transcription from smFISH for *cis* and *trans* conditions in WT, −IAA, and +IAA conditions. Each circle represents a single smFISH replicate experiment, as shown in (D) (n = 4;6;4;3;4;3, from left to right with each replicate >500 cells). Horizontal lines represent means. Significance was calculated between *cis* and *trans* for each condition. Only significant bars are shown. *p < 0.05; **p < 0.01, determined by two-tailed t test.

(F) Same as (D), for *MS2-GAL7* and *PP7-GAL10* in WT (left, n = 2,865 cells), −IAA (n = 3,815 cells), and +IAA (right, n = 4,544 cells).

(G) Same as (E), for *GAL10-GAL7* (n = 7;7;4;3;4;3, from left to right). ***p < 0.001.

See also Figures S1–S3.

for maintaining high *GAL* transcription and that transcription-generated DNA supercoiling accumulation limits subsequent transcription of neighboring genes. These inhibitory effects depend on topoisomerase concentration and gene orientation.

Degradation of topoisomerases reduces the simultaneous initiation of neighboring *GAL* genes

The refractory periods at neighboring genes upon supercoiling accumulation suggested that the divergent and tandem *GAL*

genes initiate together less often than in WT. Although the amplitude of the CCF-peak appeared to increase in topoisomerase-deficient conditions compared with WT (Figures 1D, 1F, and 2B–2F), suggesting increased co-bursting, this amplitude reflects the correlation during both active and inactive periods and is thus confounded by reduced transcriptional activity (Figure 3A). To assess co-bursting during active periods only, we quantified the normalized transcriptional overlap of *GAL1-GAL10* and *GAL10-GAL7* upon topoisomerase degradation. We observed that the overlap of *GAL1-GAL10 cis*, compared with *trans*, was reduced upon partial topoisomerase degradation (Figure 3B). Similar to the effects on the refractory periods, this loss in overlap was alleviated at full degradation conditions (Figure 3B). For *GAL10-GAL7*, the *cis* overlap progressively decreased compared with *trans* with increased degradation (Figure 3C). The reduced overlap indicated that rapid release of DNA supercoils by topoisomerases is essential to maintain coupling of the *GAL* genes.

To confirm this overlap reduction, we performed smFISH experiments after topoisomerase degradation. Similar to the live-cell experiments, topoisomerase degradation strongly reduced the transcriptional activity and transcriptionally active fraction (Figures 3D, 3F, S2P, and S2Q). However, in contrast to the transcriptional overlap measure, we noticed that the Pearson correlation is not a normalized measure but depended on transcriptional activity. In the *trans* control, with reduced transcriptional activity at partial and full degradation, we also observed a decrease in the *GAL1-GAL10* and *GAL10-GAL7* correlations (Figures 3E and 3G). Nevertheless, partial degradation significantly decreased the correlation of the *cis* compared with the *trans* for both gene pairs (Figures 3E and 3G). The decreased *GAL1-GAL10* and *GAL10-GAL7* correlations were also corroborated in untagged WT strains using gene-specific smFISH probes (Figures S3A and S3B). The basal Top1 and Top2 degradation and its associated phenotype could partially be rescued by the addition of the antagonist, auxinole, confirming the specificity of the effects (Figures S3C–S3N). These results indicate that the divergent and tandem *GAL* genes initiate together less frequently when supercoils accumulate at the locus. For the divergent genes, the reduced correlation challenges previous models, which had predicted that in eukaryotes, the accumulation of negative supercoils in divergent promoters enhances the correlation.[22–25,45] The specific reduction of the *GAL1-GAL10* overlap upon partial topoisomerase degradation (Figure 3B) instead suggests a more complicated model at this locus, where DNA supercoiling accumulation results in mutual inhibition between *GAL1* and *GAL10* and reduced simultaneous transcription.

To understand why supercoiling accumulation reduced simultaneous transcription, we focused on the transcriptional activities of the three *GAL* genes. Complete topoisomerase degradation reduced the transcription of all three genes, whereas partial topoisomerase degradation inhibited *GAL10* transcription more than *GAL1* and *GAL7* (Figure 3A). Analysis of the bursting parameters using binarized *MS2/PP7* traces revealed that topoisomerase inhibition results in shorter-duration, lower-intensity, and lower-frequency bursts for all three genes (Figures S2K–S2M). Burst intensity was already maximally affected at partial degradation (Figure S2K), but burst duration and frequency showed topoisomerase dose-dependent effects (Figures S2L and S2M), with the largest effects at *GAL10*. The uneven *GAL10* inhibition was supported by smFISH, in which the percentage of actively transcribing cells upon partial topoisomerase degradation was reduced more for *GAL10* than for *GAL1* (Figure S2P). The *GAL10* ACF also showed a prominent refractory period, which was not as evident for *GAL1* and *GAL7* (Figures S1B, S1C, S1E, and S1F). The specific inhibition of *GAL10* may explain the *GAL1-GAL10* correlation loss upon partial topoisomerase degradation. We conclude that topoisomerases ensure correlated transcription between the *GAL* gene pairs.

Transcription of *GAL7* inhibits *GAL10* transcription upon partial topoisomerase depletion

We hypothesized that the disproportionate inhibition of *GAL10* transcription upon partial topoisomerase degradation (Figure 3A) is caused by interference from the highly expressed downstream gene *GAL7*. To test this hypothesis, we used two complementary approaches to limit the possible effects of *GAL7* transcription (Figures 4A and 4B).

First, transcription of *GAL7* was abolished by scrambling both Gal4 upstream activating sequences (UASs) in the *GAL7* promoter (Figures 4A and S4A). Abrogating *GAL7* transcription in this mutant was expected to increase *GAL10* expression and therefore increase the correlation between *GAL1* and *GAL10*. As predicted, smFISH after partial and full topoisomerase degradation showed an increase in the *GAL10* active fraction (Figure S4I) and a rescue in the *GAL1-GAL10* correlation to WT (Figure 4C). Live-cell imaging of the *GAL1-GAL10* genes upon loss of *GAL7* transcription showed dampened valleys at +100 s time delay and loss of periodicity in the *GAL10* ACF and *GAL1-GAL10* CCF, revealing a weaker *GAL10* refractory period, which was most evident in the partial degradation condition (Figures 4D, 4E, and S4B–S4G). *GAL7* inhibition also partially rescued the *GAL1-GAL10* transcriptional overlap at zero time delay after partial degradation (Figure S4H). In full degradation conditions, where transcription inhibition from neighboring genes was already less evident (Figures 2C and 3B), the *GAL1-GAL10* overlap was unaffected by *GAL7* inhibition (Figure S4H). These results demonstrate that transcription of *GAL7* inhibits *GAL10* transcription when topoisomerase levels are reduced. Interestingly, in cells with WT topoisomerase levels (−OsTIR1), elimination of *GAL7* transcription did not affect the *GAL10* active fraction (Figure S4I), nor the *GAL1-GAL10* correlation (Figure 4C), suggesting that WT cells possess sufficient topoisomerase levels to prevent the inhibition of *GAL7* on *GAL10* transcription.

As a second method to test whether *GAL7* transcription inhibits *GAL10* transcription, a 1.4 kb spacer sequence was inserted between *GAL10* and *GAL7* to dissipate transcription-generated supercoils (Figure 4B). In cells with partial topoisomerase degradation, the addition of a spacer increased the *GAL10* active fraction (Figure S4J) and partially rescued the *GAL1-GAL10* correlation (Figure 4C), corroborating supercoiling-mediated inhibition of *GAL10*. Similar to the Gal4 UAS perturbation, spacer addition did not affect the *GAL1-GAL10*

CellPress
OPEN ACCESS

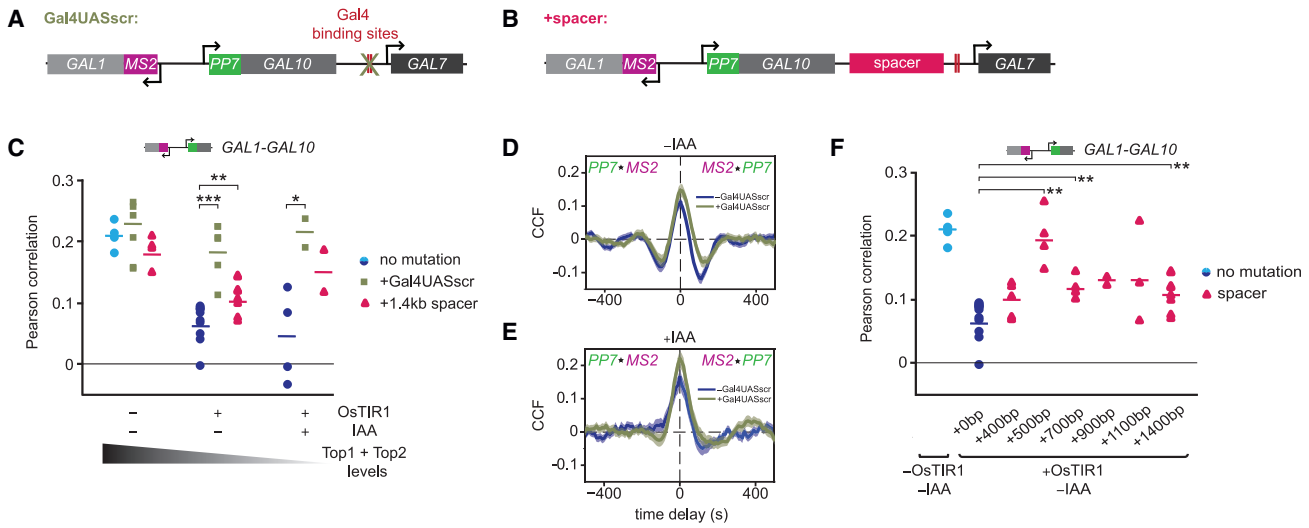

Figure 4. Transcription of *GAL7* inhibits *GAL10* transcription in partial topoisomerase degradation conditions

(A and B) Schematic of the *GAL1-GAL10 cis*-labeled locus with: (A) scrambled Gal4UAS sites (Gal4UASscr) in the *GAL7* promoter and (B) insertion of a spacer sequence in the *GAL10-GAL7* intergenic region.

(C) Pearson correlation coefficients of *GAL1-GAL10* nascent transcription from smFISH of −OsTIR (blue circles), −IAA and + IAA (navy circles) cells with Gal4UASscr (green squares) and insertion of a 1.4 kb spacer (magenta triangles). Horizontal lines represent mean. Each symbol represents a single smFISH replicate experiment (n = 4;6;4;7;6;5;4;2;2, from left to right with each replicate >500 cells). Significance was calculated between without and with Gal4UASscr/spacer for each condition. Only significant bars are shown. *p < 0.05; **p < 0.01; ***p < 0.001, determined by two-tailed t test.

(D and E) Overlay of *MS2-PP7* cross-correlation of *GAL1-GAL10* in topoisomerase-deficient cells (top, −IAA, n = 224 cells; bottom, +IAA, n = 135 cells) with Gal4UASscr (green) and with WT Gal4UAS (navy; same as Figure 2C). Shaded area indicates SEM.

(F) Same as (C) for *GAL1-GAL10* with increasing spacer sequence lengths (pink triangles) (n = 4;7;5;4;4;2;3;8).

See also Figure S4.

correlation in cells with WT topoisomerase levels (−OsTIR1) (Figure 4C). Moreover, the insertion of spacers with various lengths revealed an optimal intergenic distance of 500 bp that fully rescues the *GAL1-GAL10* correlation with partial rescues at other distances (Figure 4F). The reason for this optimal distance is unclear. Overall, these perturbations demonstrate that *GAL7* transcription inhibits *GAL10* transcription in partial topoisomerase depletion, but not in WT conditions.

Transcription inhibition at the *GAL* locus is caused by both positive and negative supercoils

We next explored how *GAL10* transcription is inhibited by *GAL7* transcription. We hypothesized that *GAL10* is inhibited either by negative supercoils traveling upstream of the *GAL7* promoter or by positive supercoils generated by *GAL10* that have limited space to dissipate while *GAL7* is being transcribed. To distinguish between these two models, we truncated the *GAL7* gene body from 1,100 to 200 bp to specifically reduce the amount of *GAL7* transcription-generated negative supercoils without changing the distance for *GAL10* supercoils to dissipate (Figure 5A). Productive transcription of the truncation was verified by smFISH (Figures S5A and S5B). In cells with WT topoisomerase levels (−OsTIR1) and with partial topoisomerase degradation, *GAL7* truncation did not affect the *GAL1-GAL10* correlation nor the *GAL1/GAL10* active fraction (Figures 5B and S5C). On full topoisomerase degradation, we observed a small rescue of the fraction of *GAL1-GAL10* transcribing cells (Figure S5C), but the correlation was not significantly changed (Figure 5B). These results suggest that upon partial degradation, *GAL10* is mainly inhibited by positive supercoils generated by its own transcription. Binding of the transcriptional machinery in the *GAL7* promoter may thus create a barrier that limits dissipation of transcription-generated positive DNA supercoils. In full-degradation conditions, negative supercoils from *GAL7* transcription may also contribute to the inhibition.

To further dissect inhibition by negative and positive supercoiling, we ectopically overexpressed bacterial topoisomerases gyrase or DNA topoisomerase I (Topo I), which selectively relieve positive or negative supercoils, respectively, and were shown to work in yeast.[31,46,47] Relieving excess positive supercoils with ectopic gyrase expression only weakly increased the *GAL10-GAL7* gene correlation in cells with WT topoisomerase levels (Figure 5D) but did not affect the correlation of *GAL1-GAL10* or *GAL10-GAL7* in partial or full topoisomerase degradation conditions (Figures 5C and 5D). In contrast, overexpression of bacterial Topo I to relax excess negative supercoils considerably increased the correlation of both gene pairs (Figures 5C and 5D). A small subpopulation exhibited higher *GAL* gene expression than WT (Figures S5F and S5G), partly explaining the increased *GAL1-GAL10* and *GAL10-GAL7* correlations. In these overexpression experiments, the timing of Topo I induction coincides with the timing of the observed effects on the correlations, arguing against possible confounding indirect effects (Figures S5D and S5E). Taken together, we conclude that at the *GAL* locus, transcription is likely inhibited by an accumulation of both negative and positive supercoils.

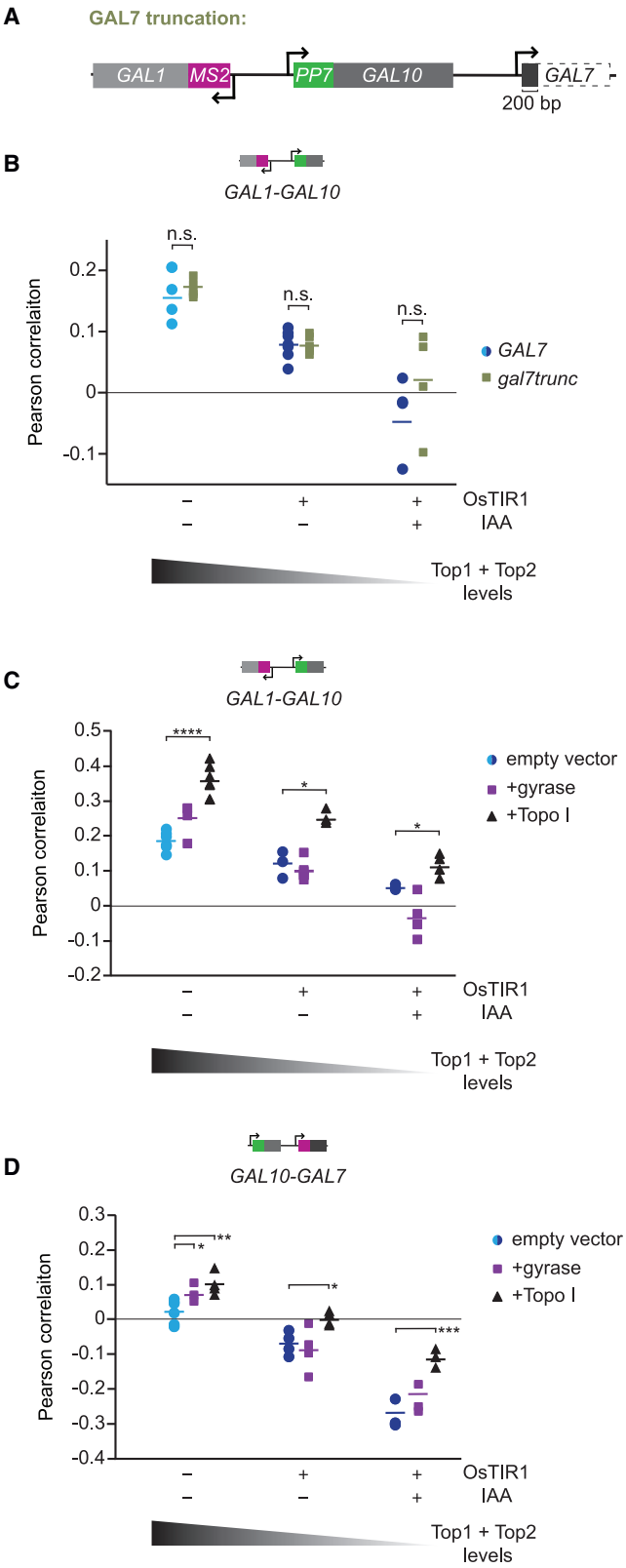

Figure 5. Transcription inhibition at the *GAL* locus is caused by both positive and negative supercoils

(A) Schematic of the *GAL1-GAL10 cis*-labeled locus with a truncation of the *GAL7* gene body from 1,100 to 200 bp.

(B) Pearson correlation coefficients of *GAL1-GAL10* nascent transcription by smFISH for WT *GAL7* (blue) and *GAL7* truncation (green) in −OsTIR1, −IAA, and +IAA cells. Each symbol represents a single smFISH replicate experiment (n = 5;5;7;5;6;4, from left to right with each replicate >500 cells). Statistical significance between WT and truncated *GAL7* was determined by two-tailed t test.

(C) Same as (B) for *GAL1-GAL10* genes with ectopic expression of gyrase (purple squares) and Topo I (black triangles) (n = 6;4;7;3;6;3;3;4;4, from left to right). Significance was calculated between empty vector and gyrase/Topo I for each condition. Only significant bars are shown. *p < 0.05; ****p < 0.0001, determined by two-tailed t test.

(D) Same as (C) for *GAL10-GAL7* (n = 6;3;4;5;4;4;3;3;3). *p < 0.05; **p < 0.01; ***p < 0.001.

See also Figure S5.

Supercoiling-mediated inhibition is caused by neither altered chromatin structures nor increased R-loops

Previous studies have shown that supercoiling accumulation can change nucleosome stability.[7,9] To gain mechanistic insight into the supercoiling-mediated transcription inhibition by nucleosome position and stability, we performed micrococcal nuclease digestion, followed by sequencing (MNase-seq) in haploid cells (Figures S6A and S6B) using high and low MNase concentrations to map stable and fragile nucleosomes, respectively.[48] Fragile nucleosomes are partially unwrapped nucleosomes, bound by the remodeler RSC (remodeling the structure of chromatin), that also occur at the Gal4 UASs in the *GAL1-GAL10* promoter.[48–50]

In partial topoisomerase degradation conditions, the position of stable and fragile nucleosomes in the *GAL* gene promoters was unchanged (Figures S6C and S6D), despite the transcription inhibition in these conditions. Only at full topoisomerase degradation did minor shifts in the nucleosome position appear at the locus, for example at the *GAL1* TATA. Similarly, only full topoisomerase degradation resulted in less well-positioned stable nucleosomes genome-wide (Figure S6E). However, since these effects were not observed on partial topoisomerase degradation, we conclude that changed nucleosome positioning or stability is not the main cause of the observed transcription inhibition on supercoiling accumulation.

Next, we reasoned that the accumulation of negative supercoils in gene bodies may lead to the formation of R-loops,[11,31,51,52] which may inhibit transcription initiation or cause premature termination. To test the influence of R-loops, we ectopically overexpressed human RNaseH (hsRNH1), which was shown to reduce R-loops in yeast.[53] Contrary to our hypothesis, resolving potential excess R-loops did not rescue the *GAL1-GAL10* correlation nor the *GAL1/GAL10* active fraction by smFISH (Figures S6F and S6G). We therefore conclude that supercoiling-mediated transcription inhibition of the *GAL* genes is caused by neither altered chromatin structures nor increased R-loops.

Accumulation of DNA supercoils reduces the Gal4 DNA residence time

Population-based ChIP measurements have suggested that DNA supercoiling accumulation reduces TF binding to DNA.[13] To investigate whether supercoiling accumulation affects the

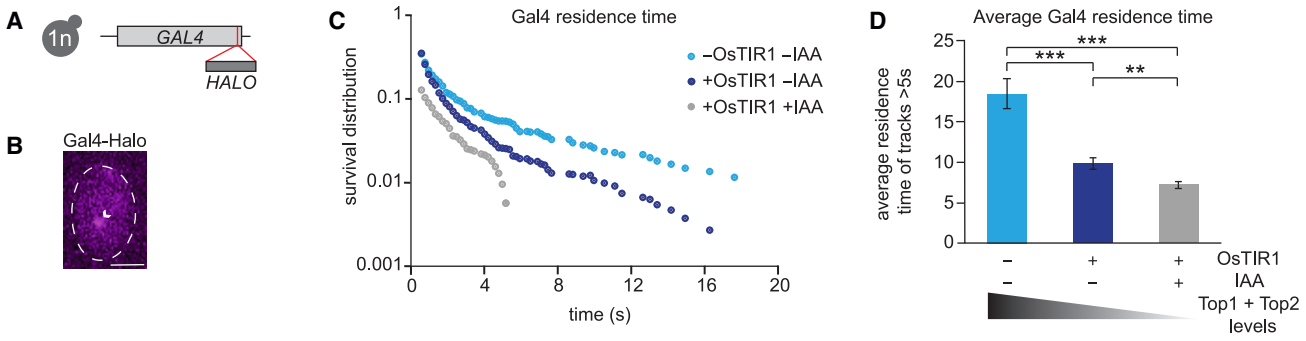

Figure 6. Supercoiling accumulation reduces the Gal4 residence time on DNA

(A) Schematic of the C-terminal HaloTag at the endogenous *GAL4* in haploid yeast (1n).

(B) Representative image of a yeast cell showing a single JFX650-labeled Gal4-HaloTag molecule (arrowhead). Scale bars, 2 μm.

(C) Survival probability distributions for Gal4 residence times in −OsTIR −IAA (323 cells, 706 tracks; 33,520 particles) and +OsTIR −IAA (244 cells, 1,378 tracks; 53,430 particles), and +OsTIR +IAA (107 cells, 187 tracks; 13,465 particles) cells.

(D) Average residence time of Gal4 calculated from trajectories with residence times >5 s for the indicated conditions. Errors indicate SEM, determined by bootstrapping with 300 repeats. **p < 0.01; ***p < 0.001.

See also Figures S6 and S7 and Video S2.

binding stability of the TF Gal4, we used single-molecule tracking (SMT) of Gal4-HaloTag to measure the DNA residence time of individual Gal4 molecules in living cells (Figures 6A and 6B). Similar to our previous measurements,[35] the semi-log survival probability distribution in WT suggested two populations with different residence times (Figure 6C). We showed that the long-bound molecules are specifically bound TFs that correlate with active transcription.[35] Comparison of the survival probability distributions between cells with decreasing topoisomerase levels revealed a progressive reduction in the Gal4 residence times (Figure 6C). Fitting of the survival distributions revealed that WT and partial topoisomerase degradation were best fit by a different function (exponential + power-law) than full degradation (biexponential) and that the fits deviated from the data at long residence times, especially after topoisomerase degradation (Figures S7A–S7C). We therefore refrained from model fitting and simply calculated the average residence time of long-bound molecules (>5 s) (Figure 6D). Partial and full topoisomerase degradation conditions exhibited shorter Gal4 residence times on the DNA. Since Gal4 residence time has been directly linked to the *GAL* gene burst duration,[35] these results suggest that the accumulation of DNA supercoils inhibit transcription by reducing the residence time of Gal4.

DNA supercoils inhibit neighboring genes of all orientations genome-wide

To understand whether supercoiling-mediated inhibition is also observed genome-wide, we performed cross-linking analysis of cDNAs, followed by sequencing (CRAC-seq) of HTP(His6-TEV-ProteinA)-tagged Rpb1, the largest subunit of RNA Pol II, to obtain high-resolution genome-wide maps of nascent transcripts for WT, partial and full degradation conditions (Figures S7D and S7E). To determine whether genes were inhibited by transcription of their neighbor, we analyzed changes in the RNA Pol II CRAC signal between partial and full topoisomerase degradation and compared both with WT (Figures S7F–S7H, also see legends). Genes were classified by the distance to the neighboring gene (Figure S7I). Genes with a close-by neighbor (100–300 bp) showed a significant downregulation on full topoisomerase degradation, which was less prominent (and less or not significant) at longer distances (>400 bp). This inhibition at longer distances is in line with the observed inhibition at the *GAL* genes for intergenic distances greater than 700 bp. However, the *GAL* genes showed a stronger supercoiling-mediated decrease in transcription than observed genome-wide, possibly due to the higher transcriptional activity and therefore likely higher DNA supercoiling production compared with most other yeast genes.[54]

To analyze whether the orientation of the neighboring gene is important for its inhibitory effect, gene pairs were grouped according to their orientations (Figure 7A). We used a threshold of 500 bp for selecting "isolated" groups, since a longer distance threshold yielded an insufficient number of gene pairs (Figure S7J). At this threshold, there was no significant difference for isolated genes without a neighbor between partial and full topoisomerase degradation, although these isolated genes were weakly but significantly downregulated, compared with WT (Figure 7B). We therefore used the partial versus full degradation comparison to analyze the different gene groups. We observed a significant downregulation in transcription for isolated gene pairs of all orientations (Figure 7B). For isolated divergent genes, transcription is likely inhibited by negative supercoils from its neighbor. For tandem pairs, both positive supercoiling and negative supercoiling may contribute to the inhibition, similar to *GAL10-GAL7*. For isolated convergent gene pairs, the most likely source of inhibition is positive supercoils. Overall, we conclude that the supercoiling-mediated inhibition observed at the *GAL* locus occurs genome-wide at neighboring genes of all orientations, providing further evidence that both positive and negative supercoiling accumulations inhibit transcription.

DISCUSSION

In this study, we combined single-molecule transcription imaging at neighboring *GAL* genes with targeted perturbations to expose

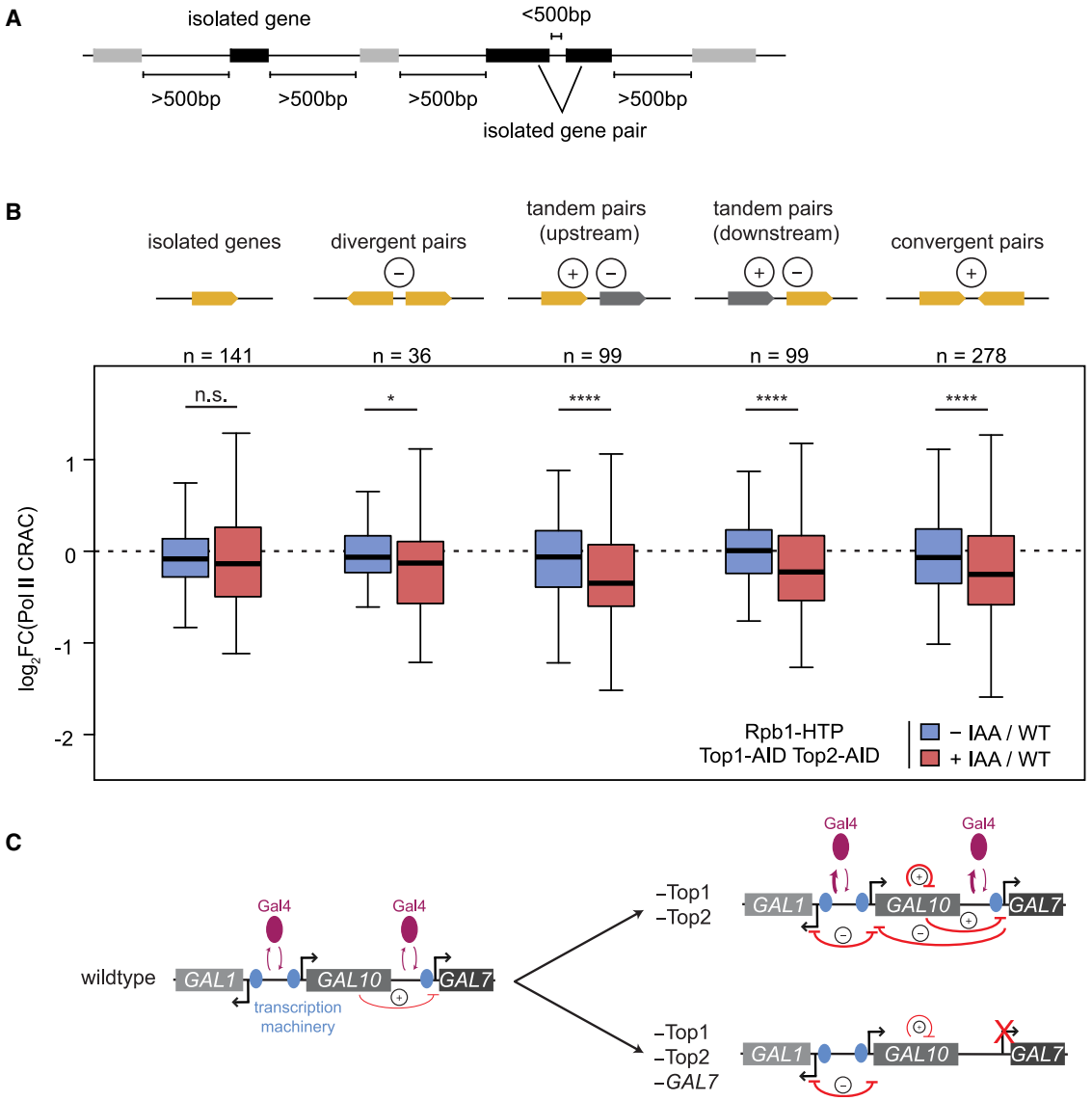

Figure 7. DNA supercoils inhibit neighboring genes genome-wide

(A) Schematic of isolated genes and gene pairs without a neighbor within 500 bp.

(B) Log_2 fold change of Rpb1 CRAC signal in −IAA and +IAA conditions, compared with WT conditions for the gene pair orientations indicated at the top. The − and + signs indicate negative and positive DNA supercoils that are expected to inhibit transcription. Gene number and significance are indicated. The box indicates quartiles, the horizontal tick line the median, and the whiskers 1.5 times the interquartile range. Significance of partial versus full topoisomerase degradation is shown: *p < 0.05; ****p < 0.0001, determined by paired t test. Significance of −IAA versus WT, from left to right: p = 0.021; p = 0.51; p = 0.042; p = 0.71; p = 0.031. Significance of +IAA versus WT, from left to right: p = 0.021; p = 0.041; p = 8.8e−6; p = 9.3e−4; p = 2.8e−6.

(C) Schematic of the proposed model. In WT (left), topoisomerase levels are sufficient to minimize supercoiling-mediated inhibition of the *GAL* genes. We only detect very weak inhibition of *GAL7* transcription, likely from positive supercoils from *GAL10* transcription. Upon topoisomerase degradation (right, top), accumulation of negative and positive supercoils from transcription inhibit transcription of neighboring genes by destabilizing binding of the transcription factor Gal4. Abrogation of *GAL7* transcription (right, bottom) removes the transcription machinery barrier in the *GAL7* promoter to allow dissipation of *GAL10* supercoils, thereby partially rescuing *GAL1-GAL10* co-bursting.

See also Figure S7.

how transcription-generated DNA supercoiling shapes transcription dynamics in budding yeast. We find that in WT, topoisomerases are sufficient to minimize supercoiling-mediated inhibition of the highly expressed *GAL* genes (Figure 7C, left). On topoisomerase degradation, the accumulation of both positive and negative DNA supercoils in the locus causes a temporally restricted expression pattern, where transcription initiation of a gene occurs simultaneously with its neighbor but is also inhibited by its neighbor during subsequent transcription events (Figure 7C, right top). This supercoiling-mediated refractory period results in a

loss of correlated transcription of the *GAL* genes. Moreover, upon partial topoisomerase degradation, *GAL10* is strongly inhibited by its own supercoils that cannot dissipate if the downstream *GAL7* gene is transcribed (Figure 7C, right bottom), further reducing simultaneous *GAL1-GAL10* transcription. Supercoiling accumulation inhibits transcription by destabilizing the binding of the TF Gal4. Overall, our data reveal that rapid supercoiling release is crucial to maintain high transcription levels and coordinate the transcription dynamics of neighboring eukaryotic genes.

In WT, transcriptional bursting of both the *GAL* gene pairs is coupled (Figures 1D and 1F). The degree of coupling is modest, but similar in magnitude to the co-bursting observed at paralogous genes in *Drosophila*.[55] Similar co-expression of closely positioned divergent genes[56–58] has fueled the prediction that negative supercoiling induces correlated transcription at neighboring genes similar to bacteria.[21,24,27,59] Although we cannot exclude that DNA supercoiling contributes by a small degree to the simultaneous initiation in WT, our data suggest that excess supercoiling at the *GAL* locus mostly impedes, rather than facilitates, transcription initiation (Figures 2, 3, and S2). Instead, we propose that coupled *GAL1-GAL10* initiation mostly originates from Gal4 binding to the shared UASs (Figure 1A). Since fluctuations in Gal4 binding directly cause fluctuations in *GAL10* transcription,[60] we expect that once Gal4 binds, it simultaneously activates *GAL1* and *GAL10*. In addition, looping or 3D proximity of the *GAL1-10* and *GAL7* promoters may facilitate correlated Gal4 binding also at the tandem *GAL* genes.[61,62] 3D interactions between shared enhancers and co-regulated promoters cause co-bursting in *Drosophila*, perhaps by allowing coordinated TF binding.[55] In line with this model, correlated TF binding has been observed for the serum response factor (SRF), resulting in correlated transcription of its target genes.[57] Finally, simultaneous transcription initiation of adjacent genes may be caused by long-distance activation of TFs, TF clustering, or TF activity gradients.[56,63–65]

At the *GAL* locus, we find that the accumulation of both positive and negative supercoiling impedes transcription. The functional relevance of this inhibition is underscored by an increase in yeast fitness when *GAL7* is relocated from the *GAL* locus to a different chromosome.[66] In prokaryotes and eukaryotes, the inhibitory role of positive supercoils is well-established[10,19,67] and is consistent with reduced genome-wide transcription of convergent and tandem genes on topoisomerase degradation (Figure 7B). Inhibition from positive supercoils is already weakly evident in WT cells at the tandem *GAL10-GAL7* genes (Figure 1F). In addition, our data suggest that transcription inhibition also occurs by negative supercoils (Figures 4D, 5C, 5D, 7B, and S5C) In line with this, in mouse embryonic stem cells, a transient accumulation of negative supercoils during base excision repair was recently found to inhibit transcription and on release, causing increased noise fluctuations.[68] The level of negative supercoiling thus requires careful regulation by topoisomerases, since low levels of negative supercoils enhance transcription,[4–6,22,45,69] but hypernegative supercoiling is inhibitory.[11,70–72] Transcription inhibition after topoisomerase degradation thus occurs through the accumulation of both positive and negative supercoils.

Positive supercoiling accumulation may inhibit transcription with a similar mechanism as in bacteria, by inhibiting both transcription initiation and elongation.[10] How negative supercoils inhibit transcription was so far less clear. Here, we observe that topoisomerase degradation reduces the residence time of Gal4 (Figure 6), as well as the burst duration of the *GAL* genes (Figure S2L). Since the Gal4 dwell time determines the burst duration,[60] it is conceivable that supercoiling-mediated transcription inhibition is caused by destabilized Gal4 binding. We envision that torsional stress in the DNA fiber from either positive or negative supercoiling results in a faster release of DNA-bound factors. Destabilization may also occur for other DNA-interacting proteins, such as factors of the preinitiation complex. Other mechanisms may also contribute to supercoiling-mediated transcription inhibition, such as small nucleosome occupancy changes on full topoisomerase degradation. Negative supercoils can cause the formation of alternative DNA structures such as Z-DNA, quadruplexes, or DNA cruciform,[73] which may limit preinitiation complex formation. Moreover, supercoils have been suggested to affect transcription post-initiation, for example, by forming excess R-loops that cause premature termination.[11,51] However, we do not find evidence for R-loop-mediated transcription inhibition or slowed elongation. We therefore propose that the DNA supercoiling at the *GAL* locus predominantly causes inhibition of transcription initiation by destabilized Gal4 binding, rather than inhibition of post-initiation steps.

Unlike in bacteria, our data suggest that in budding yeast, topoisomerases are not present at limiting concentrations for transcription dynamics. First, the refractory period observed upon topoisomerase depletion is not or only weakly present in WT (Figure 1). Second, inhibition of *GAL7* transcription or spacer addition in WT has no effect (Figure 4C). This fundamental difference in supercoiling regulation between bacteria and yeast may be the result of differences in the topoisomerase enzymes, as bacterial topoisomerases are specialized for positive or negative supercoils, whereas eukaryotic topoisomerases relieve both.[74] This difference in topoisomerase enzymes may also explain why transcription in bacteria is mostly inhibited by positive supercoils, whereas transcription in yeast is inhibited by both. In addition, eukaryotes may buffer positive supercoils by nucleosomes.[28,29] Nevertheless, our data indicate that eukaryotic topoisomerases are also not present in large excess since 25% basal degradation of topoisomerases already causes transcriptional effects. Topoisomerase levels may be tightly controlled to ensure that DNA supercoiling accumulation remains at a level that is beneficial for transcription while limiting harmful effects. The weak valleys in the *GAL10-GAL7* CCF in WT (Figure 1F) suggest that topoisomerase levels are at the tipping point of this balance.

In more complex eukaryotes, transcription-generated negative supercoils contribute to cohesin extrusion and may therefore facilitate the formation of topologically associating domains (TADs).[33,75,76] This mechanism assumes propagation of negative supercoils over much larger genomic distances than 1.5 kb, the distance at which negative supercoils were initially thought to spread.[23,77] Although mammalian genes are spaced much further apart than that in yeast, supercoiling-dependent cohesin extrusion may cause supercoiling-effects from adjacent genes at larger distances. In more complex eukaryotes, the accumulation of negative supercoils during nuclear processes,

such as base excision repair,[68] could influence the transcription of genes throughout the TAD. Overall, our single-cell live-cell approach highlights how efficient release of torsional stress is necessary to prevent transcriptional inhibition of neighboring eukaryotic genes.

Limitations of the study

The lack of methods to measure DNA supercoils in single cells has prevented us from mechanistically linking the single-cell transcription dynamics to local DNA supercoiling changes. The population-based nature of current supercoiling assays limits the interpretation for a mixed population of inactive cells, and dynamically transcribing active cells, which may cancel out any effects of positive and negative supercoils within single cells.

Additionally, bleaching and phototoxicity limited the amount of excitation light and the number of time frames during which transcription could be measured in live cells, which likely introduced a detection limit. Interpretation of noisy and short traces from individual cells was therefore challenging. The current cross-correlation approach reliably detects average enrichments or depletions but may potentially mask rare subpopulations.

Finally, the Gal4 residence times measurements represented binding events to all genomic loci, and not specifically to the *GAL* locus. Nevertheless, since Gal4 only binds to 15 genomic binding sites,[78] of which 6 are positioned at the *GAL* gene cluster, topoisomerase depletion likely reduces the Gal4 residence time at the *GAL* locus.

STAR★METHODS

Detailed methods are provided in the online version of this paper and include the following:

- KEY RESOURCES TABLE
- RESOURCE AVAILABILITY
  - Lead contact
  - Materials availability
  - Data and code availability
- EXPERIMENTAL MODEL AND SUBJECT DETAILS
  - Yeast strains, plasmids, and oligos
- METHOD DETAILS
  - Live-cell imaging of transcription dynamics
  - Single-molecule FISH
  - Western blot
  - MNase-seq
  - Single-molecule tracking of Gal4
  - CRAC-seq
- QUANTIFICATION AND STATISTICAL ANALYSIS
  - Analysis of live-cell transcription dynamics
  - ACF, CCF, and transcriptional overlap
  - smFISH analysis
  - Western blot quantification
  - Quantification of eGFP-Topo I fluorescence
  - MNase-seq analysis
  - Analysis of Gal4 single-molecule tracking
  - CRAC-seq analysis

SUPPLEMENTAL INFORMATION

Supplemental information can be found online at https://doi.org/10.1016/j.molcel.2023.04.015.

ACKNOWLEDGMENTS

We thank Bas van Steensel for helpful discussions and guidance, Fred van Leeuwen and Stefano G. Manzo for critical reading of the manuscript, and members of the T.L.L. lab for helpful feedback. We thank Evelina Tutucci for sharing the 12xMS2V6 plasmid (Addgene plasmid 104390), Daniela Delneri for the *loxP*-mutant plasmid, Benjamin Albert and David Shore for Top1-AID, Top2-AID W303 haploids, and Joaquim Roca for gyrase (pSTS77) and Topo I (YEptopA-PGAL1) plasmids. We thank David Ball for assistance with SMT analysis and the NKI Research High Performance Computing Facility and Genomics Core Facility for assistance. This work was supported by an institutional grant of the Dutch Cancer Society and of the Dutch Ministry of Health, Welfare and Sport; the Dutch Research Council (NWO, 016.Veni.192.071 and gravitation program CancerGenomiCs.nl); Oncode Institute, which is partly financed by the Dutch Cancer Society; and the European Research Council (ERC Starting grant 755695 BURSTREG). U.A. was supported by the French Ministry for Education and Research, by the Foundation ARC pour la Recherche sur le Cancer, and by the EUR G.E.N.E. (reference #ANR-17-EURE-0013), which is part of the Université Paris Cité IdEx #ANR-18-IDEX-0001 funded by the French Government through its "Investments for the Future" program.

AUTHOR CONTRIBUTIONS

Conceptualization, H.P.P. and T.L.L.; data curation, H.P.P. and U.A.; formal analysis, H.P.P., S.C., W.P., I.B., U.A., and T.L.L.; funding acquisition, I.B., T.L.L., and D.L.; investigation, H.P.P.; methodology, H.P.P. and T.L.L.; software, H.P.P., S.C., W.P., I.B., U.A., and T.L.L.; supervision, D.L. and T.L.L.; visualization, H.P.P. and T.L.L.; writing – original draft, H.P.P. and T.L.L.; writing – review & editing, H.P.P., T.L.L., S.C., W.P., I.B., U.A., and D.L.

DECLARATION OF INTERESTS

The authors declare no competing interests.

Received: April 7, 2022
Revised: February 14, 2023
Accepted: April 14, 2023
Published: May 18, 2023

REFERENCES

1. Liu, L.F., and Wang, J.C. (1987). Supercoiling of the DNA template during transcription. Proc. Natl. Acad. Sci. USA *84*, 7024–7027. https://doi.org/10.1073/pnas.84.20.7024.
2. Tsao, Y.P., Wu, H.Y., and Liu, L.F. (1989). Transcription-driven supercoiling of DNA: direct biochemical evidence from in vitro studies. Cell *56*, 111–118. https://doi.org/10.1016/0092-8674(89)90989-6.
3. Wu, H.Y., Shyy, S.H., Wang, J.C., and Liu, L.F. (1988). Transcription generates positively and negatively supercoiled domains in the template. Cell *53*, 433–440. https://doi.org/10.1016/0092-8674(88)90163-8.
4. Kouzine, F., Sanford, S., Elisha-Feil, Z., and Levens, D. (2008). The functional response of upstream DNA to dynamic supercoiling in vivo. Nat. Struct. Mol. Biol. *15*, 146–154. https://doi.org/10.1038/nsmb.1372.
5. Mizutani, M., Ohta, T., Watanabe, H., Handa, H., and Hirose, S. (1991). Negative supercoiling of DNA facilitates an interaction between transcription factor IID and the fibroin gene promoter. Proc. Natl. Acad. Sci. USA *88*, 718–722. https://doi.org/10.1073/pnas.88.3.718.
6. Parvin, J.D., and Sharp, P.A. (1993). DNA topology and a minimal set of basal factors for transcription by RNA polymerase II. Cell *73*, 533–540. https://doi.org/10.1016/0092-8674(93)90140-I.

7. Sheinin, M.Y., Li, M., Soltani, M., Luger, K., and Wang, M.D. (2013). Torque modulates nucleosome stability and facilitates H2A/H2B dimer loss. Nat. Commun. *4*, 2579. https://doi.org/10.1038/ncomms3579.

8. Tabuchi, H., Handa, H., and Hirose, S. (1993). Underwinding of DNA on binding of yeast TFIID to the TATA element. Biochem. Biophys. Res. Commun. *192*, 1432–1438. https://doi.org/10.1006/bbrc.1993.1576.

9. Teves, S.S., and Henikoff, S. (2014). Transcription-generated torsional stress destabilizes nucleosomes. Nat. Struct. Mol. Biol. *21*, 88–94. https://doi.org/10.1038/nsmb.2723.

10. Chong, S., Chen, C., Ge, H., and Xie, X.S. (2014). Mechanism of transcriptional bursting in bacteria. Cell *158*, 314–326. https://doi.org/10.1016/j.cell.2014.05.038.

11. Drolet, M. (2006). Growth inhibition mediated by excess negative supercoiling: the interplay between transcription elongation, R-loop formation and DNA topology. Mol. Microbiol. *59*, 723–730. https://doi.org/10.1111/j.1365-2958.2005.05006.x.

12. Ma, J., Bai, L., and Wang, M.D. (2013). Transcription under torsion. Science *340*, 1580–1583. https://doi.org/10.1126/science.1235441.

13. Pedersen, J.M., Fredsoe, J., Roedgaard, M., Andreasen, L., Mundbjerg, K., Kruhøffer, M., Brinch, M., Schierup, M.H., Bjergbaek, L., and Andersen, A.H. (2012). DNA topoisomerases maintain promoters in a state competent for transcriptional activation in Saccharomyces cerevisiae. PLoS Genet. *8*, e1003128. https://doi.org/10.1371/journal.pgen.1003128.

14. Roedgaard, M., Fredsoe, J., Pedersen, J.M., Bjergbaek, L., and Andersen, A.H. (2015). DNA topoisomerases are required for preinitiation complex assembly during GAL gene activation. PLoS One *10*, e0132739. https://doi.org/10.1371/journal.pone.0132739.

15. Chen, C.-C., Chou, M.-Y., Huang, C.-H., Majumder, A., and Wu, H.-Y. (2005). A cis-spreading nucleoprotein filament is responsible for the gene silencing activity found in the promoter relay mechanism. J. Biol. Chem. *280*, 5101–5112. https://doi.org/10.1074/jbc.M411840200.

16. El Hanafi, D., and Bossi, L. (2000). Activation and silencing of leu-500 promoter by transcription-induced DNA supercoiling in the Salmonella chromosome. Mol. Microbiol. *37*, 583–594. https://doi.org/10.1046/j.1365-2958.2000.02015.x.

17. El Houdaigui, B., Forquet, R., Hindré, T., Schneider, D., Nasser, W., Reverchon, S., and Meyer, S. (2019). Bacterial genome architecture shapes global transcriptional regulation by DNA supercoiling. Nucleic Acids Res. *47*, 5648–5657. https://doi.org/10.1093/nar/gkz300.

18. Rhee, K.Y., Opel, M., Ito, E., Hung, Sp., Arfin, S.M., and Hatfield, G.W. (1999). Transcriptional coupling between the divergent promoters of a prototypic LysR-type regulatory system, the ilvYC operon of Escherichia coli. Proc. Natl. Acad. Sci. USA *96*, 14294–14299. https://doi.org/10.1073/pnas.96.25.14294.

19. Sobetzko, P. (2016). Transcription-coupled DNA supercoiling dictates the chromosomal arrangement of bacterial genes. Nucleic Acids Res. *44*, 1514–1524. https://doi.org/10.1093/nar/gkw007.

20. Ancona, M., Bentivoglio, A., Brackley, C.A., Gonnella, G., and Marenduzzo, D. (2019). Transcriptional bursts in a nonequilibrium model for gene regulation by supercoiling. Biophys. J. *117*, 369–376. https://doi.org/10.1016/j.bpj.2019.04.023.

21. Brackley, C.A., Johnson, J., Bentivoglio, A., Corless, S., Gilbert, N., Gonnella, G., and Marenduzzo, D. (2016). Stochastic model of supercoiling-dependent transcription. Phys. Rev. Lett. *117*, 018101. https://doi.org/10.1103/PhysRevLett.117.018101.

22. Dunaway, M., and Ostrander, E.A. (1993). Local domains of supercoiling activate a eukaryotic promoter in vivo. Nature *361*, 746–748. https://doi.org/10.1038/361746a0.

23. Kouzine, F., Gupta, A., Baranello, L., Wojtowicz, D., Ben-Aissa, K., Liu, J., Przytycka, T.M., and Levens, D. (2013). Transcription dependent dynamic supercoiling is a short-range genomic force. Nat. Struct. Mol. Biol. *20*, 396–403. https://doi.org/10.1038/nsmb.2517.

24. Meyer, S., and Beslon, G. (2014). Torsion-mediated interaction between adjacent genes. PLoS Comput. Biol. *10*, e1003785. https://doi.org/10.1371/journal.pcbi.1003785.

25. Naughton, C., Corless, S., and Gilbert, N. (2013). Divergent RNA transcription: a role in promoter unwinding? Transcription *4*, 162–166. https://doi.org/10.4161/trns.25554.

26. Wang, G.-Z., Lercher, M.J., and Hurst, L.D. (2011). Transcriptional coupling of neighboring genes and gene expression noise: evidence that gene orientation and noncoding transcripts are modulators of noise. Genome Biol. Evol. *3*, 320–331. https://doi.org/10.1093/gbe/evr025.

27. Johnstone, C.P., and Galloway, K.E. (2022). Supercoiling-mediated feedback rapidly couples and tunes transcription. Cell Rep. *41*, 111492. https://doi.org/10.1016/j.celrep.2022.111492.

28. Bancaud, A., Wagner, G., Conde E Silva, N., Lavelle, C., Wong, H., Mozziconacci, J., Barbi, M., Sivolob, A., Le Cam, E., Mouawad, L., et al. (2007). Nucleosome chiral transition under positive torsional stress in single chromatin fibers. Mol. Cell *27*, 135–147. https://doi.org/10.1016/j.molcel.2007.05.037.

29. Bancaud, A., Conde e Silva, N., Barbi, M., Wagner, G., Allemand, J.F., Mozziconacci, J., Lavelle, C., Croquette, V., Victor, J.M., Prunell, A., et al. (2006). Structural plasticity of single chromatin fibers revealed by torsional manipulation. Nat. Struct. Mol. Biol. *13*, 444–450. https://doi.org/10.1038/nsmb1087.

30. Kaczmarczyk, A., Meng, H., Ordu, O., van Noort, J.V., and Dekker, N.H. (2020). Chromatin fibers stabilize nucleosomes under torsional stress. Nat. Commun. *11*, 126. https://doi.org/10.1038/s41467-019-13891-y.

31. Achar, Y.J., Adhil, M., Choudhary, R., Gilbert, N., and Foiani, M. (2020). Negative supercoil at gene boundaries modulates gene topology. Nature *577*, 701–705. https://doi.org/10.1038/s41586-020-1934-4.

32. Guo, M.S., Kawamura, R., Littlehale, M.L., Marko, J.F., and Laub, M.T. (2021). High-resolution, genome-wide mapping of positive supercoiling in chromosomes. eLife *10*, e67236. https://doi.org/10.7554/eLife.67236.

33. Naughton, C., Avlonitis, N., Corless, S., Prendergast, J.G., Mati, I.K., Eijk, P.P., Cockroft, S.L., Bradley, M., Ylstra, B., and Gilbert, N. (2013). Transcription forms and remodels supercoiling domains unfolding large-scale chromatin structures. Nat. Struct. Mol. Biol. *20*, 387–395. https://doi.org/10.1038/nsmb.2509.

34. Baranello, L., Wojtowicz, D., Cui, K., Devaiah, B.N., Chung, H.J., Chan-Salis, K.Y., Guha, R., Wilson, K., Zhang, X., Zhang, H., et al. (2016). RNA polymerase II regulates topoisomerase 1 activity to favor efficient transcription. Cell *165*, 357–371. https://doi.org/10.1016/j.cell.2016.02.036.

35. Lenstra, T.L., Coulon, A., Chow, C.C., and Larson, D.R. (2015). Single-molecule imaging reveals a switch between spurious and functional ncRNA transcription. Mol. Cell *60*, 597–610. https://doi.org/10.1016/j.molcel.2015.09.028.

36. Lenstra, T.L., and Larson, D.R. (2016). Single-molecule mRNA detection in live yeast. Curr. Protoc. Mol. Biol. *113*, 14.24.1–14.24.15. https://doi.org/10.1002/0471142727.mb1424s113.

37. Tutucci, E., Vera, M., Biswas, J., Garcia, J., Parker, R., and Singer, R.H. (2018). An improved MS2 system for accurate reporting of the mRNA life cycle. Nat. Methods *15*, 81–89. https://doi.org/10.1038/nmeth.4502.

38. Rodriguez, J., Ren, G., Day, C.R., Zhao, K., Chow, C.C., and Larson, D.R. (2019). Intrinsic dynamics of a human gene reveal the basis of expression heterogeneity. Cell *176*, 213–226.e18. https://doi.org/10.1016/j.cell.2018.11.026.

39. Patel, H.P., Brouwer, I., and Lenstra, T.L. (2021). Optimized protocol for single-molecule RNA FISH to visualize gene expression in S. cerevisiae. Star Protoc. *2*, 100647. https://doi.org/10.1016/j.xpro.2021.100647.

40. Sperling, A.S., Jeong, K.S., Kitada, T., and Grunstein, M. (2011). Topoisomerase II binds nucleosome-free DNA and acts redundantly with topoisomerase I to enhance recruitment of RNA Pol II in budding yeast. Proc. Natl. Acad. Sci. USA *108*, 12693–12698. https://doi.org/10.1073/pnas.1106834108.

41. Nishimura, K., Fukagawa, T., Takisawa, H., Kakimoto, T., and Kanemaki, M. (2009). An auxin-based degron system for the rapid depletion of proteins in nonplant cells. Nat. Methods *6*, 917–922. https://doi.org/10.1038/nmeth.1401.

42. Harper, C.V., Finkenstädt, B., Woodcock, D.J., Friedrichsen, S., Semprini, S., Ashall, L., Spiller, D.G., Mullins, J.J., Rand, D.A., Davis, J.R.E., et al. (2011). Dynamic analysis of stochastic transcription cycles. PLoS Biol. *9*, e1000607. https://doi.org/10.1371/journal.pbio.1000607.

43. Molina, N., Suter, D.M., Cannavo, R., Zoller, B., Gotic, I., and Naef, F. (2013). Stimulus-induced modulation of transcriptional bursting in a single mammalian gene. Proc. Natl. Acad. Sci. USA *110*, 20563–20568. https://doi.org/10.1073/pnas.1312310110.

44. Suter, D.M., Molina, N., Gatfield, D., Schneider, K., Schibler, U., and Naef, F. (2011). Mammalian genes are transcribed with widely different bursting kinetics. Science *332*, 472–474. https://doi.org/10.1126/science.1198817.

45. Kouzine, F., Liu, J., Sanford, S., Chung, H.J., and Levens, D. (2004). The dynamic response of upstream DNA to transcription-generated torsional stress. Nat. Struct. Mol. Biol. *11*, 1092–1100. https://doi.org/10.1038/nsmb848.

46. Trigueros, S., and Roca, J. (2002). Failure to relax negative supercoiling of DNA is a primary cause of mitotic hyper-recombination in topoisomerase-deficient yeast cells. J. Biol. Chem. *277*, 37207–37211. https://doi.org/10.1074/jbc.M206663200.

47. Trigueros, S., and Roca, J. (2002). A GyrB-GyrA fusion protein expressed in yeast cells is able to remove DNA supercoils but cannot substitute eukaryotic topoisomerase II. Genes Cells *7*, 249–257. https://doi.org/10.1046/j.1365-2443.2002.00516.x.

48. Kubik, S., Bruzzone, M.J., Jacquet, P., Falcone, J.-L., Rougemont, J., and Shore, D. (2015). Nucleosome stability distinguishes two different promoter types at all protein-coding genes in yeast. Mol. Cell *60*, 422–434. https://doi.org/10.1016/j.molcel.2015.10.002.

49. Brahma, S., and Henikoff, S. (2019). RSC-Associated Subnucleosomes Define MNase-Sensitive Promoters in Yeast. Mol. Cell *73*, 238–249.e3. https://doi.org/10.1016/j.molcel.2018.10.046.

50. Floer, M., Wang, X., Prabhu, V., Berrozpe, G., Narayan, S., Spagna, D., Alvarez, D., Kendall, J., Krasnitz, A., Stepansky, A., et al. (2010). A RSC/nucleosome complex determines chromatin architecture and facilitates activator binding. Cell *141*, 407–418. https://doi.org/10.1016/j.cell.2010.03.048.

51. Chedin, F., and Benham, C.J. (2020). Emerging roles for R-loop structures in the management of topological stress. J. Biol. Chem. *295*, 4684–4695. https://doi.org/10.1074/jbc.REV119.006364.

52. Kim, S., Beltran, B., Irnov, I., and Jacobs-Wagner, C. (2019). Long-distance cooperative and antagonistic RNA polymerase dynamics via DNA supercoiling. Cell *179*, 106–119.e16. https://doi.org/10.1016/j.cell.2019.08.033.

53. Aiello, U., Challal, D., Wentzinger, G., Lengronne, A., Appanah, R., Pasero, P., Palancade, B., and Libri, D. (2022). Sen1 is a key regulator of transcription-driven conflicts. Mol. Cell *82*, 2952–2966.e6. https://doi.org/10.1016/j.molcel.2022.06.021.

54. Xiong, L., Zeng, Y., Tang, R.-Q., Alper, H.S., Bai, F.-W., and Zhao, X.-Q. (2018). Condition-specific promoter activities in Saccharomyces cerevisiae. Microb. Cell Factories *17*, 58. https://doi.org/10.1186/s12934-018-0899-6.

55. Levo, M., Raimundo, J., Bing, X.Y., Sisco, Z., Batut, P.J., Ryabichko, S., Gregor, T., and Levine, M.S. (2022). Transcriptional coupling of distant regulatory genes in living embryos. Nature *605*, 754–760. https://doi.org/10.1038/s41586-022-04680-7.

56. Cohen, B.A., Mitra, R.D., Hughes, J.D., and Church, G.M. (2000). A computational analysis of whole-genome expression data reveals chromosomal domains of gene expression. Nat. Genet. *26*, 183–186. https://doi.org/10.1038/79896.

57. Ebisuya, M., Yamamoto, T., Nakajima, M., and Nishida, E. (2008). Ripples from neighbouring transcription. Nat. Cell Biol. *10*, 1106–1113. https://doi.org/10.1038/ncb1771.

58. Michalak, P. (2008). Coexpression, coregulation, and cofunctionality of neighboring genes in eukaryotic genomes. Genomics *91*, 243–248. https://doi.org/10.1016/j.ygeno.2007.11.002.

59. Sevier, S.A., and Levine, H. (2018). Properties of gene expression and chromatin structure with mechanically regulated elongation. Nucleic Acids Res. *46*, 5924–5934. https://doi.org/10.1093/nar/gky382.

60. Donovan, B.T., Huynh, A., Ball, D.A., Patel, H.P., Poirier, M.G., Larson, D.R., Ferguson, M.L., and Lenstra, T.L. (2019). Live-cell imaging reveals the interplay between transcription factors, nucleosomes, and bursting. EMBO J. *38*, e100809. https://doi.org/10.15252/embj.2018100809.

61. Lainé, J.P., Singh, B.N., Krishnamurthy, S., and Hampsey, M. (2009). A physiological role for gene loops in yeast. Genes Dev. *23*, 2604–2609. https://doi.org/10.1101/gad.1823609.

62. O'Sullivan, J.M., Tan-Wong, S.M., Morillon, A., Lee, B., Coles, J., Mellor, J., and Proudfoot, N.J. (2004). Gene loops juxtapose promoters and terminators in yeast. Nat. Genet. *36*, 1014–1018. https://doi.org/10.1038/ng1411.

63. Chong, S., Dugast-Darzacq, C., Liu, Z., Dong, P., Dailey, G.M., Cattoglio, C., Heckert, A., Banala, S., Lavis, L., Darzacq, X., et al. (2018). Imaging dynamic and selective low-complexity domain interactions that control gene transcription. Science *361*, eaar2555. https://doi.org/10.1126/science.aar2555.

64. Dobi, K.C., and Winston, F. (2007). Analysis of transcriptional activation at a distance in Saccharomyces cerevisiae. Mol. Cell. Biol. *27*, 5575–5586. https://doi.org/10.1128/MCB.00459-07.

65. Karr, J.P., Ferrie, J.J., Tjian, R., and Darzacq, X. (2022). The transcription factor activity gradient (TAG) model: contemplating a contact-independent mechanism for enhancer-promoter communication. Genes Dev. *36*, 7–16. https://doi.org/10.1101/gad.349160.121.

66. Lang, G.I., and Botstein, D. (2011). A test of the coordinated expression hypothesis for the origin and maintenance of the GAL cluster in yeast. PLoS One *6*, e25290. https://doi.org/10.1371/journal.pone.0025290.

67. Gartenberg, M.R., and Wang, J.C. (1992). Positive supercoiling of DNA greatly diminishes mRNA synthesis in yeast. Proc. Natl. Acad. Sci. USA *89*, 11461–11465. https://doi.org/10.1073/pnas.89.23.11461.

68. Desai, R.V., Chen, X., Martin, B., Chaturvedi, S., Hwang, D.W., Li, W., Yu, C., Ding, S., Thomson, M., Singer, R.H., et al. (2021). A DNA repair pathway can regulate transcriptional noise to promote cell fate transitions. Science *373*, eabc6506. https://doi.org/10.1126/science.abc6506.

69. Tabuchi, H., and Hirose, S. (1988). DNA supercoiling facilitates formation of the transcription initiation complex on the fibroin gene promoter. J. Biol. Chem. *263*, 15282–15287.

70. Baaklini, I., Usongo, V., Nolent, F., Sanscartier, P., Hraiky, C., Drlica, K., and Drolet, M. (2008). Hypernegative supercoiling inhibits growth by causing RNA degradation. J. Bacteriol. *190*, 7346–7356. https://doi.org/10.1128/JB.00680-08.

71. Dages, S., Dages, K., Zhi, X., and Leng, F. (2018). Inhibition of the gyrA promoter by transcription-coupled DNA supercoiling in Escherichia coli. Sci. Rep. *8*, 14759. https://doi.org/10.1038/s41598-018-33089-4.

72. Mizutani, M., Ura, K., and Hirose, S. (1991). DNA superhelicity affects the formation of transcription preinitiation complex on eukaryotic genes differently. Nucleic Acids Res. *19*, 2907–2911.

73. Bacolla, A., and Wells, R.D. (2004). Non-B DNA conformations, genomic rearrangements, and human disease. J. Biol. Chem. *279*, 47411–47414. https://doi.org/10.1074/jbc.R400028200.

74. Pommier, Y., Sun, Y., Huang, S.-Y.N., and Nitiss, J.L. (2016). Roles of eukaryotic topoisomerases in transcription, replication and genomic stability. Nat. Rev. Mol. Cell Biol. *17*, 703–721. https://doi.org/10.1038/nrm.2016.111.

75. Racko, D., Benedetti, F., Dorier, J., and Stasiak, A. (2018). Transcription-induced supercoiling as the driving force of chromatin loop extrusion during formation of TADs in interphase chromosomes. Nucleic Acids Res. *46*, 1648–1660. https://doi.org/10.1093/nar/gkx1123.

76. Neguembor, M.V., Martin, L., Castells-García, Á., Gómez-García, P.A., Vicario, C., Carnevali, D., AlHaj Abed, J., Granados, A., Sebastian-Perez, R., Sottile, F., et al. (2021). Transcription-mediated supercoiling regulates genome folding and loop formation. Mol. Cell *81*, 3065–3081.e12. https://doi.org/10.1016/j.molcel.2021.06.009.

77. Racko, D., Benedetti, F., Dorier, J., and Stasiak, A. (2019). Are TADs supercoiled? Nucleic Acids Res. *47*, 521–532. https://doi.org/10.1093/nar/gky1091.

78. Rhee, H.S., and Pugh, B.F. (2011). Comprehensive genome-wide protein-DNA interactions detected at single-nucleotide resolution. Cell *147*, 1408–1419. https://doi.org/10.1016/j.cell.2011.11.013.

79. Challal, D., Barucco, M., Kubik, S., Feuerbach, F., Candelli, T., Geoffroy, H., Benaksas, C., Shore, D., and Libri, D. (2018). General regulatory factors control the fidelity of transcription by restricting non-coding and ectopic initiation. Mol. Cell *72*, 955–969.e7. https://doi.org/10.1016/j.molcel.2018.11.037.

80. Grimm, J.B., Xie, L., Casler, J.C., Patel, R., Tkachuk, A.N., Falco, N., Choi, H., Lippincott-Schwartz, J., Brown, T.A., Glick, B.S., et al. (2021). A general method to improve fluorophores using deuterated auxochromes. JACS Au *1*, 690–696. https://doi.org/10.1021/jacsau.1c00006.

81. Schneider, C.A., Rasband, W.S., and Eliceiri, K.W. (2012). NIH Image to ImageJ: 25 years of image analysis. Nat. Methods *9*, 671–675. https://doi.org/10.1038/nmeth.2089.

82. Langmead, B., and Salzberg, S.L. (2012). Fast gapped-read alignment with Bowtie 2. Nat. Methods *9*, 357–359. https://doi.org/10.1038/nmeth.1923.

83. Mazza, D., Ganguly, S., and McNally, J.G. (2013). Monitoring dynamic binding of chromatin proteins in vivo by single-molecule tracking. Methods Mol. Biol. *1042*, 117–137. https://doi.org/10.1007/978-1-62703-526-2_9.

84. Love, M.I., Huber, W., and Anders, S. (2014). Moderated estimation of fold change and dispersion for RNA-seq data with DESeq2. Genome Biol. *15*, 550. https://doi.org/10.1186/s13059-014-0550-8.

85. Laughery, M.F., Hunter, T., Brown, A., Hoopes, J., Ostbye, T., Shumaker, T., and Wyrick, J.J. (2015). New vectors for simple and streamlined CRISPR-Cas9 genome editing in Saccharomyces cerevisiae. Yeast Chichester Engl. *32*, 711–720. https://doi.org/10.1002/yea.3098.

86. Brouwer, I., Patel, H.P., Meeussen, J.V.W., Pomp, W., and Lenstra, T.L. (2020). Single-molecule fluorescence imaging in living Saccharomyces cerevisiae Cells. Star Protoc. *1*, 100142. https://doi.org/10.1016/j.xpro.2020.100142.

87. Edelstein, A.D., Tsuchida, M.A., Amodaj, N., Pinkard, H., Vale, R.D., and Stuurman, N. (2014). Advanced methods of microscope control using μManager software. J. Biol. Methods *1*, e10. https://doi.org/10.14440/jbm.2014.36.

88. de Jonge, W.J., O'Duibhir, E., Lijnzaad, P., van Leenen, D., Groot Koerkamp, M.J., Kemmeren, P., and Holstege, F.C. (2017). Molecular mechanisms that distinguish TFIID housekeeping from regulatable SAGA promoters. EMBO J. *36*, 274–290. https://doi.org/10.15252/embj.201695621.

89. Candelli, T., Challal, D., Briand, J.-B., Boulay, J., Porrua, O., Colin, J., and Libri, D. (2018). High-resolution transcription maps reveal the widespread impact of roadblock termination in yeast. EMBO J. *37*, e97490. https://doi.org/10.15252/embj.201797490.

90. Coulon, A., Ferguson, M.L., De Turris, V., Palangat, M., Chow, C.C., and Larson, D.R. (2014). Kinetic competition during the transcription cycle results in stochastic RNA processing. eLife *3*, 1–22. https://doi.org/10.7554/eLife.03939.

91. Fu, X., Patel, H.P., Coppola, S., Xu, L., Cao, Z., Lenstra, T.L., and Grima, R. (2022). Quantifying how post-transcriptional noise and gene copy number variation bias transcriptional parameter inference from mRNA distributions. eLife *11*, e82493. https://doi.org/10.7554/eLife.82493.

92. Garcia, D.A., Fettweis, G., Presman, D.M., Paakinaho, V., Jarzynski, C., Upadhyaya, A., and Hager, G.L. (2021). Power-law behavior of transcription factor dynamics at the single-molecule level implies a continuum affinity model. Nucleic Acids Res. *49*, 6605–6620. https://doi.org/10.1093/nar/gkab072.

STAR★METHODS

KEY RESOURCES TABLE

REAGENT or RESOURCE	SOURCE	IDENTIFIER
Antibodies		
IgG from rabbit serum	Sigma-Aldrich	Cat# I5006; RRID: AB_1163659
c-Myc polyclonal	Thermo Fischer Scientific	Cat# PA5-85185; RRID: AB_2792331
PGK1 monoclonal	Thermo Fischer Scientific	Cat# 459250;RRID: AB_2532235
IRDye® 800CW anti-mouse	Li-cor	Cat# 925-32210; RRID: AB_2687825
IRDye® 800CW anti-rabbit	Li-cor	Cat# 926-32211; RRID: AB_621843
Chemicals, peptides, and recombinant proteins		
Yeast Nitrogen Base w/o AA, Carbohydrate & w/ AS (YNB) (Powder)	US Biological	Cat# Y2025
Drop-out Mix Complete w/o Yeast Nitrogen Base (Powder)	US Biological	Cat# D9515
Bacto™ Agar	Thermo Fischer Scientific	Cat#214030
Bacto™ Peptone	Thermo Fischer Scientific	Cat# 211677
Bacto™ Yeast Extract, technical	Thermo Fischer Scientific	Cat# 288620
D-Glucose	Sigma-Aldrich	Cat# 8270-10KG
D-Raffinose	Bio-Connect Life Sciences	Cat# OR06197_2kg
D-Galactose	Sigma-Aldrich	Cat# G0750-500G
1× Tris-EDTA buffer pH 8.0	Invitrogen	Cat# 12090015
D-Sorbitol	Sigma-Aldrich	Cat# S6021
Potassium phosphate monobasic (powder)	Sigma-Aldrich	Cat# P9791
Potassium phosphate dibasic (powder)	Sigma-Aldrich	Cat# P8281
B-Mercaptoethanol	Sigma-Aldrich	Cat# M6250
Lyticase from *Arthrobacter luteus* (powder)	Sigma-Aldrich	Cat# L2524
Ribonucleoside Vanadyl Complex (RVC; liquid)	NEB	Cat# S1402S
Formamide (deionized)	Sigma-Aldrich	Cat# F9037
UltraPure™ SSC, 20X	Thermo Fisher Scientific	Cat# 15557044
Dextran sulfate sodium salt	Sigma-Aldrich	Cat# 67578
ProLong® Gold Antifade Mountant with DAPI	Invitrogen	Cat# P36935
Sodium chloride (NaCl)	Sigma-Aldrich	Cat# S9888
Glycerol	Sigma-Aldrich	Cat# G5516
Phosphate-buffered saline (PBS)	Thermo Fisher Scientific	Cat# 18912014
MyTaq Red Mix 2x	Bioline	Cat#: BIO-25044
DMSO	Sigma	Cat#: D4540
DNase I recombinant, RNase-free	Sigma-Aldrich (Roche)	Cat# 04716728001
cOmplete EDTA-free protease inhibitor cocktail tablets	Sigma-Aldrich (Roche)	Cat# 11873580001
Pefabloc SC-Protease-Inhibitor	Carl Roth	Cat# A154.3
Dynabeads M-280 Tosylactivated	Thermo Fisher Scientific	Cat# 14204
RNace-It Ribonuclease Cocktail	Agilent	Cat# 400720
Recombinant GST-TEV protease	Challal et al.[79]	N/A
Guanidine hydrochloride	Sigma-Aldrich	Cat# G4505
Ni-NTA Agarose	Qiagen	Cat# 30230
Imidazole	Sigma-Aldrich	Cat# I0125

(*Continued on next page*)

Continued

REAGENT or RESOURCE	SOURCE	IDENTIFIER
RNaseOUT Recombinant Ribonuclease Inhibitor	Thermo Fisher Scientific	Cat# 10777019
T4 RNA Ligase 2, truncated KQ	NEB	Cat# M0373L
T4 Polynucleotide Kinase	NEB	Cat# M0201L
T4 RNA Ligase 1 (ssRNA Ligase)	NEB	Cat# M0204L
Proteinase K, recombinant, PCR grade	Sigma-Aldrich (Roche)	Cat# 03115887001
SuperScript IV Reverse Transcriptase	Thermo Fisher Scientific	Cat# 18090050
Exonuclease I	NEB	Cat# M0293S
RNase H	NEB	Cat# M0297S
LA Taq	Takara	Cat# RR002M
Zymolase 100T	US biological	Cat# Z1004.250
Micrococcal nuclease	Sigma-Aldrich	Cat# N5386-200UN
Sorbitol	Sigma Aldrich	Cat# 1077581000
Ammonium acetate solution	Sigma Aldrich	Cat# A2706
NP-40	Sigma Aldrich	Cat# 92016
SDS	Sigma Aldrich	Cat# L3771
Spermidine	Sigma Aldrich	Cat# S0266
Phenol/chloroform (PCI 15:14:1)	Sigma-Aldrich	Cat# P2069-100ML
RNaseA/T1	Thermo Fisher Scientific	Cat# EN0551
Agarose MP	Sigma Aldrich	Cat# 11388991001
3-indole acetic acid (IAA, auxin)	Sigma Aldrich	Cat# I3750-100G-A
NuPAGE™ SDS Running buffer 20x	Thermo Fisher Scientific	Cat# LA0041
NuPAGE™ 3-8%Tris-Acetate protein gels	Thermo Fisher Scientific	Cat#EA0375PK2
Nitrocellulose membrane	Bio-rad	Cat# 1620112
Auxinole	Sigma Aldrich	Cat# SML3231-25MG
JFX650 dye	Grimm et al.[80]	N/A
Critical commercial assays		
LightCycler FastStart DNA Master SYBR Green I	Roche	Cat# 12239364001
LightCycler 480 SYBR Green I Master	Roche	Cat# 04887352001
Qubit dsDNA HS Assay Kit	Thermo Fisher Scientific (Invitrogen)	Cat# Q32851
Vivacon 500	Sartorius	Cat# VN01H22
QIAquick PCR Purification Kit	Qiagen	Cat# 28104
PCR Isolate II PCR and Gel Kit	Bioline	Cat# BIO-52060
Bioanalyzer High Sensitivity DNA kit	Agilent	Cat# 5067-4626
ISOLATE II Plasmid Mini Kit	Bioline	Cat# BIO-52057
KAPA HTP Library Preparation Kit	KAPA Biosystems	Cat# 07961901001
Deposited data		
MNase-seq data	this study	GEO: GSE196945
Pol II CRAC-seq	this study	GEO: GSE217963
Raw images and Western blots	this study	Mendeley Data: https://doi.org/10.17632/z2w34669gj.1
Experimental models: Organisms/strains		
Please refer to Table S1	this study	N/A
Oligonucleotides		
Please refer to Tables S3, S4, and S5	this study	N/A
Recombinant DNA		
Please refer to Table S2	this study	N/A

(*Continued on next page*)

Continued

REAGENT or RESOURCE	SOURCE	IDENTIFIER
Software and algorithms		
ImageJ	Schneider et al.[81]	https://imagej.nih.gov/ij/index.html
Python	custom code	https://doi.org/10.5281/zenodo.7820986 https://doi.org/10.5281/zenodo.7820895 https://doi.org/10.5281/zenodo.7820931 https://doi.org/10.5281/zenodo.7821005
Bowtie2	Langmead and Salzberg[82]	http://bowtie-bio.sourceforge.net/bowtie2/index.shtml
MATLAB (MatTrack v6)	Mazza et al.,[83] kind gift from David Ball	https://doi.org/10.5281/zenodo.7821136
DESeq2	Love et al.[84]	https://bioconductor.org/packages/release/bioc/html/DESeq2.html
RStudio	RStudio	RRID: SCR_000432
Affinity Designer	Serif	https://affinity.serif.com/en-us/designer/; RRID: SCR_016952
Other		
"Megatron" W5 UV crosslinking unit	UVO3 Ltd	https://www.uvo3.co.uk/
Mixer Mill MM 400	Retsch	Cat# 20.745.0001
Gelfree 8100 Fractionation Station	Expedeon	Cat# 48100
18 mm round cover slips coated with poly-L-lysine	Neuvitro	Cat# GG-18-1.5-pll
25mm round cover glasses (#1.5, thickness)	VWR	Cat# 631-0172
25mm round cover glasses HI D=0.17m	Zeiss	Cat# 000000-1787-996
Wash-N-Dry coverslip rack	Sigma Aldrich	Cat# Z688568-1EA
400 mL tall glass beakers	Novodirect	Cat# 15439093
Microscope slides, SuperFrost®	VWR	Cat# ISO8037/I
Attofluor™ Cell Chamber, for microscopy	Thermofisher Scientific	Cat# A7816
Dumont Horlogemakers pincet Gebogen Nr. 7 (forceps, tweezers)	Vos Medisch	Cat# 1121
Cell density meter	VWR	Cat#634-0882
Parafilm® M (4 inches wide)	Merck	P7668
Zeiss Plan-Apochromat 40×/1.40NA Oil	Zeiss	Cat# 420762-9900-000
Zeiss 4-alpha Plan-Apochromat 100×/1.46NA Oil	Zeiss	Cat# 420792-9800-000
Zeiss alpha Plan-Apochromat 100x 1.57NA oil	Zeiss	Cat# 420792-9771-000
SPECTRA X light engine WL:360–680 nm	Lumencor	N/A
ORCA Flash 4v3 digital sCMOS camera	Hamamatsu	Cat# C13440-20CU
UNO Top stage incubator and objective heater	Okolab	N/A
Excitation filters, emission filters and dichroic mirrors	See method details	N/A

RESOURCE AVAILABILITY

Lead contact

Further information and requests for resources and reagents should be directed to and will be fulfilled by the lead contact, Tineke L. Lenstra (t.lenstra@nki.nl).

Materials availability

Plasmids and yeast strains generated in this study are available upon reasonable request from the lead contact with a completed Materials Transfer Agreement.

Data and code availability

- The sequencing (MNase-seq and Pol II CRAC-seq) data from this publication have been deposited and are publicly available as of the date of publication. Accession numbers and DOI are listed in the key resources table. Microscopy data is available upon request.
- All original code for the live-cell, smFISH, SMT and MNase-seq analysis has been deposited to Zenodo. DOI are listed in the key resources table.
- Any additional information required to reanalyze the data reported in this paper is available from the lead contact upon request.

EXPERIMENTAL MODEL AND SUBJECT DETAILS

Yeast strains, plasmids, and oligos

Haploid yeast cells (*Saccharomyces cerevisiae*) of BY4741 and BY4742 backgrounds were transformed and mated to obtain the BY4743 diploids listed in Table S1. 12xMS2V6 loops were integrated at 5' *GAL1* with a PCR product containing loxP-kanMX-loxP and at 5' *GAL7* with loxP2272-kanMX-loxP2272, a loxP mutant to prevent recombination with WT loxP sequence. The kanMX was excised with inducible CRE recombinase. Plasmids containing the MS2 and PP7 coat proteins, fused to mScarlet and GFPEnvy, respectively (pTL174 and pTL333), were digested with PacI and integrated at the *ura3Δ0* locus. Auxin-inducible degron tags at *TOP1* and *TOP2* were amplified from YTL738 or pTL398 and integrated at the endogenous loci. Plasmid containing OsTIR1 (pTL231) was digested with PacI and integrated at the *his3Δ1* locus. Gal4UASscr, *GAL7* truncation and spacer mutations were made using CRISPR/Cas9.[85] The spacer sequence included convergent ADH1t and CUT60t terminator sequences to prevent transcriptional interference. All integrations were checked with PCR and sequencing. Gyrase and Topo I were ectopically expressed from plasmids. smFISH experiments with gene-specific probes upon topoisomerase degradation and CRAC-seq experiments were performed in haploid cells with W303 background. Cells were grown at 30°C in synthetic media. Strains, plasmids and oligos used to construct the strains can be found in Tables S1, S2, and S3, respectively.

METHOD DETAILS

Live-cell imaging of transcription dynamics

Live-cell imaging of transcription dynamics was performed as previously described in Donovan et al.[60] and Brouwer et al.[86] with minor modifications. Cells were grown at 30°C for at least 14 h in synthetic complete media supplemented with 2% raffinose. The cells were imaged after 30 min galactose induction at 30°C at mid-log (optical density, OD_{600} 0.2–0.4) on a coverslip with an agarose pad consisting of synthetic complete media and 2% galactose. For indole-3-acetic acid (IAA; auxin) treatment, cells were treated with galactose for 30 min and with 500 μM for 15 min before imaging. For auxinole treatment, cells were grown for at least 14 h in 500 μM auxinole and induced with galactose for 30 min before imaging.

Imaging was performed on a setup consisting of an inverted microscope (Zeiss AxioObserver), an alpha Plan-Apochromat 100x 1.46NA oil objective, an sCMOS camera (Hamamatsu ORCA Flash 4v3) with a dual bandpass dichroic (Chroma 59012bs), a 570 nm longpass beamsplitter (Chroma T565lpxr-UF1), and 515/30 and 600/52 emission filters (Semrock FF01-515/30-25 and Semrock FF01-600/52-25), an UNO Top stage incubator and objective heater (OKOlab) at 30°C, LED excitation at 470/24 nm and 550/15 nm (SpectraX, Lumencor) at 0.20% and 0.40% power with an ND2 filter, resulting in a 62 mW/cm^2 and 413 mW/cm^2 excitation intensity. Wide-field images of GFPEnvy and mScarlet signals were acquired sequentially to prevent spectral crosstalk. Images were recorded at 10s interval for 30 min, with 9 *z*-stacks (Δz 0.5 μm) and 200 ms exposure using the Micro-Manager software, version 1.4.[87] For each condition, at least 3 replicate datasets were acquired with a total at least 100 cells.

Single-molecule FISH

Yeast cultures were grown to mid-log (OD_{600} 0.5) in 25 mL synthetic complete media with 2% raffinose and 2% galactose and smFISH was performed as previously described with minor modifications.[39,60] For auxinole treatment, cells were grown in synthetic complete media with 500 μM auxinole and 2% galactose. For the auxin timepoints, 100mL cultures were grown to OD_{600} 0.4 before being divided into 4×25 mL cultures and treated with 500 μM auxin for specified amount of time before fixation. If timepoint is not specified, cells were treated with auxin for 60 min. Cells were harvested at the same time after auxin addition to ensure the same OD.

Cells were fixed with 5% paraformaldehyde (Electron Microscopy Sciences, 15714-S) for 20 min, washed three times with buffer B (1.2 M sorbitol and 100 mM potassium phosphate buffer pH 7.5) and then spheroplasted with 300 units of lyticase (Sigma-Aldrich, L2524-25KU). Cells were then immobilized on poly-L-lysine-coated coverslips (Neuvitro) and permeabilized with 70% ethanol. Coverslips were hybridized for 4 h at 37°C with hybridization buffer containing 10% dextran sulfate, 10% formamide, 2×SSC, and 5 pmol of fluorescent probes. For FISH targeting the PP7 and MS2 repeats, four PP7 probes labeled with Quasar570 and 48 MS2 probes labeled with Quasar670 dyes were used. For FISH targeting *GAL1*, *GAL10* or *GAL7*, 48 probes labeled with Quasar570 (*GAL1* and *GAL7*) or Quasar670 (*GAL10*) were used (Table S4). Coverslips were washed 2× for 30 min with 10% formamide, 2×SSC at 37°C, then 1× with 2×SSC, and 1× for 5 min with PBS at room temperature. Coverslips were mounted on microscope slides using ProLong Gold mounting media with DAPI (Thermo Fisher, P36934).

Imaging was performed on two similar microscopes consisting of an inverted microscope (Zeiss AxioObserver), a Plan-Apochromat 40x 1.4NA oil DIC UV objective, a 1.60x optovar, and an sCMOS camera (Hamamatsu ORCA Flash 4v3). For Quasar570, a 562 nm longpass dichroic (Chroma T562lpxr), 595/50 nm emission filter (Chroma ET595/50m) and 550/15 nm LED excitation at full power (Spectra X, Lumencor) were used. For Quasar670, a 660 nm longpass dichroic (Semrock FF660-Di02-25x36 or Chroma T660lpxrxt), 697/60 nm emission filter (Chroma ET697/60m) and 640/30 nm LED excitation at full power (Spectra X, Lumencor) were used. For DAPI, either a 410nm/490nm/570nm/660nm dichroic (Chroma vcgr-spx-p01-PC), a 430/35 nm, 512/45 nm, 593/40 nm, 665 nm longpass emission filter (Chroma vcgr-spx-p01-EM) or a 425 nm longpass dichroic (Chroma T425lpxr) and a 460/50 nm emission filter (Chroma ET460/50m) and LED excitation at 395/25 nm at 25% power (Spectra X, Lumencor) were used. For each sample and each channel, we utilized the Micro-Manager software, version 1.4 to acquire at least 50 fields-of-view, each consisting of a 21 *z*-stack (Δz 0.3 μm) at 25 ms exposure for DAPI and 250 ms exposure for Quasar570 and Quasar670. For the smFISH experiments with the untagged topoisomerase-deficient haploids, all imaging settings were the same except a 1.25× optovar was used and each field-of-view consisted of 13 *z*-stack (Δz 0.5 μm).

Western blot

Yeast cultures were grown to mid-log (OD_{600nm} 0.4) in 25 mL synthetic complete media with 2% raffinose and 2% galactose. For auxinole treatment, cells were grown in synthetic complete media with 500 μM auxinole and 2% galactose. The cells were treated with 500 μM auxin for 15, 30, or 60 min. Cells were harvested at the same time to ensure the same OD. Cells were washed with PBS twice and then incubated in 200 mM NaOH for 10 min. The cells were pelleted and resuspended in 2× SDS-PAGE solvent (4% SDS, 20% glycerol, 0.1 M DTT, 0.125 M Tris-HCl pH 7.5 and Roche EDTA-free protease inhibitor cocktail) and boiled at 95°C for 5min. The lysates were centrifuged, the supernatant was collected and snap-frozen in liquid nitrogen and stored at −80°C.

To determine the loading volume, samples were first checked with a dot blot. The same WT control strain was used to ensure similar loading between experiments. For the western blot, samples were run on a 3-8% Tris-acetate gel (Thermo Fisher Scientific, EA0375PK2) at 100V for 2 hours and wet transferred (Bio-Rad, 1703930) on a nitrocellulose membrane at 300 mA for 4 hours. The membrane was washed with PBS for 5 min, blocked with 5% milk, dissolved in PBS, for 1 h at 18-22°C and incubated in 2% milk dissolved in TBS-T containing 1:1000 dilution of anti-cMyc (Thermo Fisher Scientific, #MA1-980) or anti-PGK (Thermo Fisher Scientific, #PA5-28612) primary antibodies, at 4°C for 14 hours. The membrane was washed with PBS for 5 min three times and incubated with 2% milk dissolved in TBS-T containing fluorescent anti-mouse (LI-COR, 926-32210) or anti-rabbit (LI-COR, 926-32211) secondary antibodies for 1 h at 18-22°C in the dark.

MNase-seq

Preparation and analysis of mono-nucleosomal DNA was performed as described previously[60,88] with minor modifications and with two biological replicates. Haploid cells were grown in synthetic complete media with 2% raffinose or 2% galactose from OD_{600} 0.3 to OD_{600} 1.0, fixed in 1% paraformaldehyde, washed with 1 M sorbitol, treated with spheroplasting buffer (1M sorbitol, 1 mM β-mercaptoethanol, 10 mg/mL zymolyase 100T (US biological, Z1004.250)) and washed twice with 1 M sorbitol. Spheroplasted cells were treated with 0.01171875 or 0.1875 U micrococcal nuclease (Sigma-Aldrich, N5386-200UN) in digestion buffer (1 M sorbitol, 50 mM NaCl, 10 mM Tris pH 7.4, 5 mM $MgCl_2$, 0.075% NP-40, 1 mM β-mercaptoethanol, 0.5 mM spermidine) at 37°C. After 45 min, reactions were terminated on ice with 25 mM EDTA and 0.5% SDS. Samples were treated with proteinase K for 1 h at 37°C and decrosslinked overnight at 65°C. Digested DNA was extracted with phenol/chloroform (PCI 15:14:1), precipitated with NH_4-Ac, and treated with 0.1 mg/mL RNaseA/T1. The extent of digestion was checked on a 3% agarose gel.

Sequencing libraries were prepared using the KAPA HTP Library Preparation Kit (07961901001, KAPA Biosystems) using 1 mg of input DNA, 5 mL of 10 mM adapter, double-sided size selection before and after amplification using 10 cycles. Adapters were created by ligation of the Universal adapter to individual sequencing adapters (Table S5). Libraries were checked on Bioanalyzer High Sensitivity DNA kit (Agilent) and sequencing was performed on a NextSeq550.

Single-molecule tracking of Gal4

Cells were grown at 30°C for at least 14 h in synthetic complete media, supplemented with 2% raffinose and 2% galactose. At mid-log (optical density, OD_{600} 0.2–0.4), cells were treated with 5 pM (H3-HaloTag cells) or 500 pM (Gal4-HaloTag cells) of JFX650 dye[80] and incubated at 30°C for 15 minutes. The cells were washed with warm media and immobilized on a coverslip with an agarose pad consisting of synthetic complete media with 2% raffinose and 2% galactose.

The cells were imaged on ELYRA.P1 (Zeiss) equipped with an incubator (Pecon) and Scanning Stage Piezo 130x100 (Zeiss). We used an alpha Plan-Apochromat 100x 1.57NA oil objective (Zeiss) and a filter set (Zeiss LBF 405/488/642). The cells were excited simultaneously with Highly Inclined Laminated Optical (HILO) sheet illumination mode with 488 nm and 640 nm using 1.6 W/cm^2 and 2 mW/cm^2 excitation intensities, respectively. Images were captured with 30 ms exposure at 200 ms interval for 1,000 time points. The emission was split in two channels (TV1 and TV2) using a duolink splitter (Zeiss) holding a filter set with a BS642 dichroic beamsplitter (Zeiss) and BP495–550 and LP655 emission filters (Semrock) onto two EM-CCD iXon DU 897 cameras (Andor).

CRAC-seq

For Pol II CRAC experiments, 2 L per condition of cells with endogenously HTP-tagged RBP1 and AID-tagged TOP1, TOP2 genes were grown to exponential phase in synthetic media lacking tryptophane at 30°C and harvested at OD600 = 0.6. Depletion of Top1-AID and Top2-AID was induced by treatment with 5 mM auxin for 1 hour before harvesting. Processing of the CRAC-seq data was performed as previously described in Candelli et al.[89] and Challal et al.[79]

QUANTIFICATION AND STATISTICAL ANALYSIS

Statistical details for individual experiments have been provided in the figure legends.

Analysis of live-cell transcription dynamics

For image analysis of transcription dynamics, the intensity calculation and tracking of the transcription sites was calculated as previously described in Donovan et al.[60] using a custom Python script (https://doi.org/10.5281/zenodo.7820895 with dependencies from https://doi.org/10.5281/zenodo.7820931). The images were maximum intensity projected and then corrected for *xy*-drift in the stage using an affine transformation. Cells were segmented using Otsu thresholding and watershedding. The intensity of the TS was calculated for each color by fitting a 2D Gaussian mask after local background subtraction as described previously.[90] To detect the TSs, initial intensity thresholds of 9 and 7 standard deviations (SD) from the mean background was used for *PP7* and *MS2* signals, respectively. For frames where no TS was detected, a second fit was made in the vicinity of the initial detected spots using lower intensity thresholds of 6 and 4 SD from the mean background for *PP7* and *MS2*, respectively. If no TSs were detected in a frame after the second fit, the intensity was measured at the *xy*-coordinates of the previous frame. The tracking within each cell was inspected visually, and the endpoint of each trace was manually set at the last frame where a TS was visible. Dividing cells and cells in which TSs were not reliably detected were excluded from the analysis. Only the cells that exhibited both *PP7* and *MS2* signals were considered for analysis. Cells with only signal in one channel were inspected but exhibited insufficient coat protein levels in the other channel for reliable analysis. For each cell, the background was estimated by fitting a Lorentzian distribution to intensities measured at four points at a fixed distance from the TS in each frame in the same cell. The mean background was subtracted from the intensity trace to obtain background-subtracted intensity traces. Active fraction was computed by accounting for cells that exhibited both PP7 and MS2 signals for at least 600 seconds. Cells where we did not detect transcription sites above background were classified as inactive.

To determine the on and off periods, the fluorescence signal was binarized by setting a threshold that was a specific standard deviation above the *MS2* and *PP7* background intensities. To determine a binarization threshold that captured the correct bursting kinetics, the sum of squared residuals between the ACFs of the binary signals (range 1.0-5.0, steps of 0.25) and the ACF of the analog fluorescence signal between 10s and 100s was calculated. The minimal residual was found at threshold values of 2.75 and 4.50 standard deviations above background, with residuals of 0.0025 and 0.0010 for *MS2* and *PP7*, respectively. The burst intensity was measured for frames where the binarized signal was on. The burst duration and burst frequency (defined as inverse of time between bursts) were calculated from the binarized data, and bursts with a duration of a single frame were considered as errors from the binarization and were excluded. Reported error bars and significance was calculated from bootstrapping with 1000 repetitions.

ACF, CCF, and transcriptional overlap

For each time trace, autocorrelation (ACF) and crosscorrelation functions (CCF) were computed as

$$G_{ab}(\tau) = \frac{\langle \delta a(t)\delta b(t+\tau)\rangle}{\langle a(t)\rangle\langle b(t)\rangle} - 1 \qquad \text{(Equation 1)}$$

where $<\cdot>$ denotes the time average, $\delta a(t) = a(t) - \langle a(t)\rangle$ and $a(t)$ and $b(t)$ can be combinations of the *MS2* and *PP7* time traces.[60,90] Correlation functions were computed using fast Fourier transforms and upon shifting the two signals, non-overlapping ends were trimmed. The functions were normalized for each trace individually. To correct for non-stationary effects (i.e. photobleaching, cell cycle, etc.), the global mean signal was used to calculate corrections, which were then subtracted. For single-trace correlation functions, each point was given a weight corresponding to the number of overlapping time intervals (τ) from the signals used in its computation. Correlation functions from single time traces were averaged together to reach statistical convergence. Bootstrapping was performed with 10,000 repetitions to obtain standard error of the mean correlation functions (SEM).

We used the ACFs and CCFs to calculate the normalized transcriptional overlap (called fractional overlap by Rodriguez et al.),[38] which provides an estimate of the fraction of bursts of one gene, which co-occur with the bursts of another gene. We normalized the cross-correlation functions of the *GAL1-GAL10* and *GAL10-GAL7* genes by their respective ACFs:

$$G_{ab}/a(\tau) = \frac{G_{ab}(\tau)+1}{G_a(0)+1} \qquad \text{(Equation 2)}$$

where $G_{ab}(\tau)$ represents the CCFs of *GAL1-GAL10* or *GAL10-GAL7*. $G_a(0)$ represents the ACF amplitude at $\tau = 0$ of *GAL10* in *GAL1-GAL10* or *GAL10-GAL7* pair. Each trace was normalized before the traces were averaged together.

To estimate the amplitude of the CCF at $\tau = 0$, we fit the CCF with a Gaussian. The measured ACF amplitude at $\tau = 0$ is overestimated due to shot noise, so to estimate the representative amplitudes $G_a(0)$ and $G_b(0)$, we fit a line through the first 4 to 10 (omitting $\tau = 0$) values of G_a and G_b. The fit with the best coefficient of determination was used to extrapolate the values of $G_a(0)$.

Rodriguez et al. presented the transcriptional overlap calculation for a model with assumptions that the transcriptional events are square pulses of equal duration and height and are uniformly distributed over time. To confirm that this calculation can be applied for bursts with trapezoidal transcription events that are exponentially distributed, we simulated a 4-state model (ON-ON, ON-OFF, OFF-ON, OFF-OFF) for a gene pair where the promoter states are correlated, similar to *GAL1-GAL10*. We find that at lower transcription rates, the calculated normalized transcriptional overlap deviates from the theoretical values. However, for highly correlated gene pairs, as observed in the real data, the calculated transcriptional overlap from Equation 2 matches the theoretical transcriptional overlap between the two genes.

smFISH analysis

For smFISH image analysis, a custom-written Python script was used to detect, localize, and classify the spots (https://doi.org/10.5281/zenodo.7820986 with dependencies from https://doi.org/10.5281/zenodo.7820931). Cells and nuclei were segmented using Otsu thresholding and watershedding. Spots were localized by fitting a 3D Gaussian mask after local background subtraction.[90] Cells in which no spots were detected were excluded from further analysis since a visual inspection indicated that these cells were not properly segmented or were improperly permeabilized. For each cell, the TS was defined as the brightest nuclear spot and the number of RNAs at each TS was determined by normalizing the intensity of each TS with the median fluorescent intensity of the cytoplasmic RNAs detected in all cells. Cells were further subclassified based on their cell cycle stage using the integrated DAPI intensity of each cell calculated from the maximum intensity projection images.[91] A distribution of nuclear DAPI intensities was fit with a bimodal Gaussian model. The TS intensity was only analyzed in G1 cells, with nuclear intensities [1 SD, 0.75× SD] around the mean of the first peak.

Cells with fewer than 5 RNAs at the TS were classified as inactive, and cells with 5 or more RNAs at the TS were classified as active cells. Subsequently, the fraction of active cells for each gene and the Pearson correlation coefficients of the active cells were determined for various conditions. For smFISH experiments with *GAL10*, *GAL1*, and *GAL7* probes, spots were fit using 2D fitting, and the threshold to classify as an active cell was set to 2.5.

Western blot quantification

The fluorescence signal of Western blots was quantified using ImageJ.[81] A region of interest (ROI) was outlined around the largest sample and the same ROI was used for all samples on the membrane. The background was calculated by averaging the intensities of eight ROIs on the membrane where there was no signal present. The integrated intensities of the samples were background-subtracted and normalized to a no-OsTIR1 control strain to determine degradation upon OsTIR1 addition and auxin addition.

Quantification of eGFP-Topo I fluorescence

To quantify the Topo I-eGFP fluorescence, cells were segmented using Otsu thresholding and watershedding. The fluorescence of each pixel within the cell was integrated and subtracted by the mean background of the image. The background was defined as the pixels unoccupied by the cell masks. The background-subtracted intensities were normalized by the area of the cell.

MNase-seq analysis

MNase-seq was analyzed with a custom python script (https://doi.org/10.5281/zenodo.7821005). Paired-end 2×75-bp reads were aligned to the reference genome SacCer3 using Bowtie 2.[82] Nucleosome dyads were found by taking the middle of each paired read of insert size between 95 and 225 bp and were smoothed with a 31-bp window.[88] The minimal read-length of 95 bp ensured inclusion of subnucleosomal particles (fragile nucleosomes) rather than regulatory factors, which is especially important when using low MNase digestion conditions.

To determine the position of the +1 nucleosome for each gene, the coverage was determined in a 4000 bp window around the annotated TSS. For each gene, the coverage was summed and smoothed using a Gaussian filter with 40 bp window. The peaks were determined using a peak calling function. The +1 nucleosome was defined as the first peak after the minimum of the smoothed coverage. To compute the metagene plot, genes were aligned at the +1 nucleosome based on classifications in the unperturbed condition and the coverages were summed and normalized by the number of genes.

Analysis of Gal4 single-molecule tracking

Single-molecule tracking movies were analyzed using a custom MATLAB software based on MatTrack (version 6, https://doi.org/10.5281/zenodo.7821136).[60,83] Dividing cells were excluded from the analysis. To determine the region of interest for the analysis, the nucleus was labeled with PP7 coat protein, fused to GFPEnvy to aid segmentation. The Gal4-HaloTag labeling density is such that 1-2 molecule were labeled in each nucleus, making it unlikely to have multiple labeled molecules in one position. Only molecules that were tracked in more than 4 frames were considered to be bound. To determine whether a molecule was bound or diffusing, a threshold was used based on tracking of histone H3. Tracking of histone H3 showed that 99% of single molecules had a frame-to-frame displacement of < 0.35 μm at 200 ms interval. These maximum displacements were used to determine whether

Gal4 particles are chromatin bound or diffusing. The cumulative distribution of dwell times of bound Gal4 molecules (survival probability plot) was corrected for bleaching based on the photobleaching kinetics of the bound histone population.[92] Briefly, the histone (H3-HaloTag) SMT data, acquired using the same conditions as Gal4-HaloTag SMT data, is fitted to a family of exponentials and the exponential distribution of the longer component is used to normalize the Gal4-HaloTag survival. The residence time distributions were computed from the photobleaching-corrected survival distributions and the average was calculated for bound tracks that were greater than 5 s in duration.

CRAC-seq analysis

Computational analyses of the CRAC-seq experiments were performed with ad hoc scripts in the R Studio environment. Differential gene expression analyses were carried out using the DESeq2 package.[84] The wildtype condition presented in Figure S7 was previously published in Aiello et al.[53]